



1 **Aerosol meteorology and Philippine receptor observations of Maritime Continent aerosol**
2 **emissions for the 2012 7SEAS southwest monsoon intensive study**

3
4 Jeffrey S. Reid¹, Nofel D. Lagrosas², Haflidi H. Jonsson³, Elizabeth A. Reid¹, Samuel A.
5 Atwood⁴, Thomas J. Boyd⁵, Virendra P. Ghatge⁶, Peng Lynch⁷, Derek J. Posselt⁸, James B.
6 Simpas², Sherdon N. Uy², Kimo Zaiger⁹, Donald R. Blake¹⁰, Anthony Bucholtz¹, James R.
7 Campbell¹, Boon Ning Chew¹¹, Steven S. Cliff¹², Brent N. Holben¹³, Robert E. Holz¹⁴, Edward J.
8 Hyer¹, Sonia M. Kreidenweis⁴, Arunas P. Kuciauskas¹, Simone Lolli¹⁵, Min Oo¹⁴, Kevin D.
9 Perry¹⁶, Santo V. Salinas¹¹, Walter R. Sessions^{7,14}, Alexander Smirnov¹⁷, Annette L Walker¹,
10 Qing Wang³, Liya Yu¹⁸, Jianglong Zhang¹⁹, Yongjing Zhao¹²

11
12 [1] {Marine Meteorology Division, Naval Research Laboratory, Monterey CA}

13 [2] {Manila Observatory, Manila Philippines}

14 [3] {Department of Meteorology, Naval Postgraduate School, Monterey CA}

15 [4] {Dept. of Atmospheric Science, Colorado State University, Ft. Collins, CO}

16 [5] {Biogeochemistry Section, Naval Research Laboratory, Washington DC}

17 [6] {Argonne National Laboratory, Argonne, IL, USA}

18 [7] {CSC Inc. at Naval Research Laboratory, Monterey CA}

19 [8] {Dept. of Atmospheric, Oceanic, and Space Sciences, University of Michigan, Ann Arbor,
20 MI}

21 [9] {NAVFAC Engineering and Expeditionary Warfare Center Port Hueneme, CA}

22 [10] {Dept. of Chemistry, University of California, Irvine, CA}

23 [11] {Centre for Remote Imaging Sensing and Processing, National University
24 of Singapore, Singapore}

25 [12] {Department of Applied Science, University of California Davis, CA}

26 [13] {NASA Goddard Space Flight Center, Greenbelt MD}

27 [14] {Space Sciences Engineering Center, University of Wisconsin, Madison, WI}

28 [15] {University of Maryland Baltimore County-JCET, Baltimore, MD}

29 [16] {University of Utah, Salt Lake City, UT}

30 [17] {Sigma Space Corporation, Lanham, MD}

31 [18] {Dept. of Environmental Engineering, National University of Singapore, Singapore}

32 [19] {Dept. of Meteorology, University of North Dakota, Grand Forks, ND}

33

34 Correspondence to: J. S. Reid (jeffrey.reid@nrlmry.navy.mil; 1 831-656-4725)

35

36



37 ABSTRACT:

38 The largest 7 Southeast Asian Studies (7-SEAS) operations period within the Maritime Continent
39 occurred in the 2012 August-September biomass burning season. Included were an enhanced
40 deployment of Aerosol Robotic Network (AERONET) sun photometers, of multiple lidars, and
41 of a Singapore supersite. Simultaneously, a ship was dispatched to the Palawan Archipelago and
42 Sulu Sea of the Philippines for September 2012 to observe transported smoke and pollution as it
43 entered the southwest monsoon monsoonal trough. Here we describe the nature of the overall
44 2012 southwest monsoon biomass burning season, but focus on the findings of the research
45 cruise and the aerosol meteorology of this convectively active region. This 2012 cruise followed
46 a 2 week cruise in 2011, and was in part consistent with the findings of that cruise for how
47 smoke emission and transport relate to monsoonal flows, the propagation of the Madden Julian
48 Oscillation (MJO), tropical cyclones, and covariance between smoke transport events and the
49 atmosphere's thermodynamic structure. Aerosol observations in the 2011 cruise also highlighted
50 the importance of squall lines and cold pools as they propagate across the South China Sea,
51 scavenging aerosol particles in their path. For 2012, the cruise experienced differing
52 environments. The monsoonal flow direction was perturbed by easterly waves, leading at times
53 to total flow reversal in the South China Sea. Two category 5 typhoons just east of the
54 Philippines also modulated flow patterns and convection. Whereas in 2011 large synoptic scale
55 aerosol events transported high concentrations of smoke into the Philippines over days, in 2012,
56 measured aerosol events exhibited a much more short term variation, sometimes only over 3-12
57 hours. Navy Aerosol Analysis and Prediction System (NAAPS) simulations captured longer
58 wavelength aerosol events quite well, but largely failed to capture the timing in high frequency
59 phenomena. Also observed were nucleation events in cleaner and polluted conditions, as well as
60 in urban plumes. Combined, observations indicate pockets of high particle counts are not
61 uncommon in the region. Perhaps most interestingly, several cases of squall lines heralding
62 major aerosol events were observed, as opposed to the previous observations in 2011 of these
63 lines largely scavenging aerosol particles from the marine boundary layer. We hypothesize that
64 these phenomena may originate from weakly forced convection ahead of polluted land breeze
65 fronts caught in strong monsoonal flows. Ultimately, the research findings of the 2012 cruise
66 nicely complement the narrative started by the 2011 research cruise, and point to the importance
67 of small scale phenomena such as sea breezes and squall lines embedded in the large scale
68 monsoonal flow patterns in dominating aerosol lifecycle and potentially effects. "Pure" biomass
69 burning plumes are relatively rare and are usually mixed with significant amounts of
70 anthropogenic pollution.

71



72 1.0 INTRODUCTION AND BACKGROUND

73 The 7 Southeast Asian Studies (7SEAS) program has motivated observation and analysis of
74 aerosol/meteorology interactions in the Maritime Continent (MC) that have led to significant
75 advances in understanding the life cycle of aerosol particles in this region. While linkages
76 between biomass burning to the El Nino Southern Oscillation (ENSO) have long been identified
77 (e.g., Nichol 1998; Field and Shen 2008), the relative importance of the Madden Julian
78 Oscillation (MJO), equatorial waves, tropical cyclones and even features as fine as boundary
79 layer dynamics and the sea breeze have been recently connected (e.g., Reid et al., 2012; 2015;
80 Atwood et al., 2013; Campbell et al., 2013; Wang et al., 2013; Xian et al., 2013; Ge et al., 2014).
81 Yet the complexity of MC meteorology continues to pose great challenges to quantitative
82 characterization and prediction of MC atmospheric composition and potential climate impacts.
83 Based on the early findings of the Coordinate Regional Climate Downscaling Experiments
84 (CORDEX; <http://www.cordex.org/>; Giorgi et al., 2012), climate model simulations for the
85 Southeast Asian domain diverge widely and have strong biases in regard to temperature and
86 precipitation. At the same time, large uncertainties in diagnosed precipitation estimates have been
87 identified based on the challenges of extrapolating across a complicated meteorological regime
88 (Jamandre and Narisma, 2013). Atmospheric models have difficulty representing complex
89 tropical waves in the MC, on scales ranging from Kelvin waves through the Madden Julian
90 Oscillation and the regional monsoon (e.g. Misra and Li, 2014; Zhang, 2014). Near ubiquitous
91 cloud cover hampers many aspects of remote sensing observation (Reid et al., 2013; Campbell et
92 al., 2016). Field measurements in the MC are difficult to obtain and quality assure. Ultimately,
93 the complexity and high degree of variability of the MC aerosol environment poses great
94 challenges in determining how aerosol particles, weather, and climate interact.

95

96 The 7SEAS program was formed in the late 2000's to enhance communication between scientists
97 interested in Southeast Asian aerosol impacts on weather and climate (Reid et al., 2013; Lin et al.
98 2013). 7SEAS quickly developed into a grass-roots organization, with a strong focus on
99 collecting information on aerosol properties and lifecycle in a region with limited data. Central
100 to this effort were studies that employed surface observations to verify and interpret satellite
101 remote sensing data, which in turn was assimilated into, or used to evaluate, models. In this
102 manner, 7SEAS allowed for some of the first end-to-end aerosol lifecycle studies in Southeast



103 Asia, and in the MC in particular. Persistent observations across the region suggest a natural
104 boundary between the regions' boreal spring northeast monsoon and summer/fall southwest
105 monsoon. 7SEAS data collection and analysis also tended to follow these monsoonal lines, with
106 one component emphasizing the springtime Peninsular Southeast Asia biomass burning season of
107 Myanmar, Thailand, Laos and Cambodia with Vietnam and Taiwan as receptors (e.g., see review
108 Lin et al., 2013), and another component emphasizing the MC.

109

110 Although all seasons are of interest, within the MC, 7SEAS field measurements and lifecycle
111 studies have focused on the August through October biomass burning season in Indonesia and
112 Malaysia, with Singapore and the Philippines as key receptors (e.g., Reid et al., 2012; 2015;
113 Atwood et al., 2013; Chew et al., 2011; 2013; Salinas et al., 2013; Xian et al., 2013; Wang et al.,
114 2013; Yang et al., 2013). Enhanced deployments of Aerosol Robotic Network (AERONET;
115 Holben et al., 1998) sun photometers to the MC began in 2007 (Salinas et al., 2009), followed by
116 the development of a Singapore based supersite (Atwood et al., 2013) and long term installations
117 of MicroPulse Lidar Network (MPLNET) lidars in 2009. Each year, progressively more
118 instrumentation or intensive measurement initiatives were added to the region. This
119 measurement effort reached a crescendo in the summer of 2012, where a series of additional sun
120 photometers, lidars and other aerosol instruments were deployed to the MC in an above-average
121 biomass burning year.

122

123 Included in the 2012 deployment was a research cruise by the M/Y *Vasco*, a 35 m Philippine
124 flagged vessel to study aerosol properties on the edge of the southwest monsoonal trough.
125 Studied were "natural" particles, as well as biomass burning and industrial emissions, being
126 transported from Indonesia, Malaysia and Singapore into the eastern South China and Sulu Seas.
127 The *Vasco* has previously been used in support of 7SEAS in late September 2011, performing a
128 research cruise in the northern Palawan Archipelago (~11° N; 119° E) and sampling two major
129 aerosol events originating from Borneo and Sumatra (Reid et al., 2015). This 2011 cruise was a
130 trial for the more substantial 2012 effort described here, and provided the means to conduct a
131 detailed seasonal examination of how biomass burning emissions and lifecycle related to tropical
132 waves. Together, these two cruises provide the first ever, to our knowledge, measurements of
133 aerosol properties in the remote southwest monsoon Southeast Asia region, increasing our



134 understanding of their relation to regional meteorology and transport patterns.

135

136 Findings of the 2011 cruise were consistent with the conceptual analysis of MC aerosol lifecycle
137 in the monsoonal flow, as put forth by Reid et al. (2012) with supported mesoscale simulations
138 by Wang et al., (2013). In particular, the 2011 cruise highlighted the role of the Madden Julian
139 Oscillation (MJO) in regulating aerosol emissions and transport. While relationships between
140 the MJO and aerosol loadings have long been hypothesized (e.g., Tian et al., 2008; Beegum et
141 al., 2009; Reid et al., 2012), these research cruises were direct verification of what was occurring
142 in observed environments under the clouds. The 2011 cruise showed that incorporated into the
143 MJO signal was the associated tropical cyclone (TC) cyclogenesis relationship put forth by
144 Maloney and Hartman (2001). Reid et al. (2012) and Wang et al. (2013) suggested that this
145 relationship strongly influences the development of aerosol events advecting into the South
146 China and Sulu Seas. Indeed, these TCs were in large part responsible for modulating
147 monsoonal flows and large scale aerosol transport during the 2011 cruise. Further, the 2011
148 *Vasco* cruise highlighted the importance of finer-scale features such as squall lines in regulating
149 over-ocean wet deposition. Ultimately, a key finding of the 2011 cruise was that while
150 monsoonal scale flow patterns and convection are important, short-lived phenomena can strongly
151 modulate cloud condensation nuclei (CCN) concentrations, resulting in pockets of clean and
152 polluted air that are difficult to account for in both observational and modeling studies of aerosol
153 interaction. The demonstrated covariance of thermodynamic structure and aerosol properties in
154 convective environments highlighted the need for any study of aerosol, cloud, and precipitation
155 interaction to control for meteorological factors.

156

157 The 2012 research cruise continues the narrative set forth from the previous year. In this paper,
158 we provide an overview of the 2012 biomass burning season and the observations of the
159 September 2012 research cruise. A description of the cruise track, instrumentation, and overall
160 sampled aerosol environment is given. As in the previous paper covering the 2011 cruise, an
161 overview of the overall aerosol and meteorological environment for 2012 is provided for context.
162 Results will focus on the relationships between observed aerosol and meteorological patterns,
163 along with a discussion of the implications for aerosol observability and predictability. Details
164 on aerosol microphysics will be provided in related papers-notably Atwood et al. (2016, to be



165 submitted) delves deeply into variability in variability in particle size distributions. While the
166 two-week 2011 cruise occurred at a location and during a period that fit nicely with conceptual
167 models and numerical model simulations, the aerosol and meteorology of the 2012 cruise was
168 more far reaching, with many high-frequency events observed that were not well simulated in the
169 models used in previous studies. The 2011 and 2012 data are compared in detail in the
170 discussion section.

171

172 2.0 CRUISE INSTRUMENTATION, TRACK, AND SUPPORTING DATA

173 The 4-29 September 2012 research cruise was conducted on the same vessel with largely the
174 same instrumentation and measurement configuration as the 2011 cruise (Reid et al., 2015). The
175 vessel used was the Cosmix Underwater Research Ltd M/Y *Vasco*, a 186 ton/35 m ship used for
176 regional diving applications, including salvage, tourism and research. However, the cruise was
177 12 days longer in duration and ventured further south, as far as Balabac Island on the southern tip
178 of the Palawan Archipelago (7.6 N; 117.0 E) that was less than 100 km from the northern tip of
179 Borneo (Figure 1 (a)). Details on the *Vasco* and its instrumentation can be found in Reid et al.,
180 (2015), although a brief overview and notable changes are described below. This is followed by
181 further descriptions of the cruise track and sampling, and finally of the ancillary data used in this
182 analysis.

183

184 2.1 *Vasco* Instrumentation

185 Instrumentation for 2012 largely mimicked 2011. A bow mast provided high-rate sampling at 50
186 Hz for turbulent fluxes using a Campbell CSAT3 3-D sonic anemometer and LI-COR H₂O/CO₂
187 gas analyzer. An Inertial Measurement Units (IMU) consisting of a GPS, a gyro stabilized
188 electronic compass, and accelerometers are used to characterize the ship position and
189 orientations for ship motion removal from the turbulence measurements. Mean meteorological
190 measurements were made by an RM Young propeller anemometer, a Campbell ventilated
191 temperature and humidity probe and a barometer for static pressure. Duplicate measurements for
192 mean meteorology and precipitation were made by a Vaisala Weather Transmitter WXT520 for
193 quality assurance purposes. Differences between all sensors for temperature was within 0.3°C,
194 RH within 5%, pressure within 0.5 hPa, and within 0.5 m s⁻¹ for winds. Downwelling short and
195 longwave radiation was measured by Kipp and Zonen CMP 22 and CGR4 instruments,



196 respectively. Cloud cover was monitored via a Vaisala C31 ceilometer. InterMet 1-AB
197 radiosondes were released two to three times a day when the ship was at a moorage. New to the
198 2012 cruise was an OTT Parsivel disdrometer for the measurement of rain rate and droplet size
199 distribution.

200

201 Atmospheric composition measurements made on the bow also largely mimicked the 2011
202 cruise. PM_{2.5} filters were collected by 5 lpm Minivol Tactical Air Samplers (TAS), and analyzed
203 by gravimetric, XRF and ion chromatography at the Desert Research Institute. A second set of
204 filters was analyzed for organic and black carbon, by the thermal-optical method of Chow et al.
205 (1993). The period of filter sampling ranged from one to two-and-a-half days depending on
206 estimated aerosol concentration. Size-resolved elemental data from Na through Pb was provided
207 by XRF analysis at the Lawrence Berkeley Lab Advanced Light Source (ALS) on samples
208 collected by an 8 stage Davis Rotating-drum Uniform size-cut Monitor (DRUM) sampler
209 (unheated PM10 inlet and cut points at 5 µm, 2.5 µm, 1.15 µm, 0.75 µm, 0.56 µm, 0.34 µm, 0.26
210 µm, and 0.07; Cahill et al., 1985). Due to an electronics failure during ship installation, this
211 instrument was manually rotated to provide data during specific periods. While total mass
212 concentrations are still in analysis, we have high confidence in PM1 elemental ratios presented in
213 this paper. As in Reid et al. (2015), sulfur, potassium, and vanadium ratios are used as markers
214 to help separate industrial anthropogenic from biomass burning particles. For trace-gas analysis,
215 95 whole-air gas samples were collected for gas chromatography analysis by the University of
216 California Irvine (See Colman et al. 2001 for a list of 60+ compounds provided, details on
217 analysis methods and relative uncertainties). Of these, 85 passed internal quality assurance tests.

218

219 Aerosol microphysics instrumentation was located in a forward locker fed by a 3 cm diameter/4
220 m long inlet from the top of the ship. Wind directional data were used to ensure that only
221 periods with air moving over the bow were used to remove periods of contamination and self-
222 sampling from the dataset. Periods of residual self-sampling were also abundantly clear from
223 CN and total particle counts. Like the previous cruise, a base set of aerosol scattering,
224 absorption number and size were made and processed by two TSI three wavelength (450, 550,
225 700 nm) nephelometers (Anderson et al., 1996) one ambient and one heated dry (50% RH), a
226 Radiance Research three wavelength (440 nm, 523 nm, 660 nm) Particle Soot Aerosol



227 Photometer (PSAP; Bond et al. 1999), TSI Condensation Nuclei Counter (CPC), a combined
228 DMT bench top Passive Cavity Aerosol Sizing Spectrometer (PCASP) and a TSI Aerodynamic
229 Particle Sizer (APS; Reid et al., 2006) for fine and coarse mode particle sizing, respectively. A
230 Maritime Aerosol Network Microtops hand-held sun photometer (MAN; Smirnov et al., 2011)
231 was brought on board for measuring Aerosol Optical Thickness (AOT) on those rare cloud free
232 occasions that permitted solar observation.

233

234 More significant additions were made to 2012 cruise relative to 2011 in regard to aerosol
235 microphysics. First, data from previous campaigns showed that the lab-bench PCASP
236 instrument was prone to calibration drift, and so a second PCASP configured in an aviation pod
237 and heated inlet was placed on the *Vasco* top mast in a manner as described in Reid et al. (2006).
238 This instrument proved to be much more reliable and steadfast in calibration of the two, and
239 hence is used in this paper's analysis. Also supplementing particle size in 2012 was a combined
240 electrostatic classifier cloud condensation nucleation counter (CCNc) package to measure the
241 size-resolved CCNc characteristics of aerosol particles. This system and its analysis are
242 described in detail in Atwood et al. (2016; to be submitted) but are summarized here. This
243 system provided aerosol particle size distributions and hygroscopicities across a size range of 17-
244 500 nm using a size-resolved CCN system similar to Petters et al. (2009). Coarse-mode particles
245 were first removed using a URG cyclone with an approximate 1 μm and 50% size cut before
246 being dried using a Permapure poly-tube Nafion column. Approximately 1.1 lpm was drawn
247 through a TSI 3080 Electrostatic Classifier with a 0.071 cm orifice impactor (approximate 0.69
248 μm 50% cutpoint diameter) and Model 3081 long DMA column, with a sheath air flow rate of 5
249 lpm for 30 bin midpoint sizes between 17 and 500 nm in diameter. Sampled air was then split
250 between a TSI 3782 Water Condensation Particle Counter (CPC) with a flow rate of 0.6 lpm, and
251 a DMT CCN Counter (CCNc) with a flow rate of 0.5 lpm. The CCN counter was operated at
252 five supersaturation set points between 0.14% and 0.85% and was calibrated using Ammonium
253 Sulfate. Calibration and inversion of the raw measured data followed the procedures described
254 by Petters et al. (2009). Number concentrations for both the CPC and CCNc counter were
255 corrected using actual flows measured by a Gilibrator. Hygroscopicity was assessed with the
256 kappa parameter (Petters and Kreidenweis, 2007) using three-parameter activated fraction fits
257 similar to Rose et al. (2010).



258

259 Finally, in parallel to the PSAP, multi-spectral absorption was measured with the newly-
260 developed NOAA Continuous Light Absorption Aerosol Photometer (CLAP). The CLAP is a
261 filter-based system of similar configuration to the PSAP, although with seven sequential filters
262 loaded that eliminates the need for frequent filter changes. Its design requirements were driven
263 by the high sensitivity necessary to monitor aerosol absorption in more pristine conditions at
264 Global Atmospheric Watch stations. Both laboratory and field comparisons between the CLAP
265 and PSAP show that they agree to within 10% (John Ogren, *NOAA manuscript in preparation*).
266 For the 2012 cruise, the CLAP was integrated with the dry nephelometer.

267

268 *2.2 Vasco Cruise Track and Sampling Schedule*

269 The *Vasco* cruise track in mid-cruise is superimposed on a MODIS Terra image in Figure 1 (a).
270 Like the previous cruise, the *Vasco* home ported from Navotas, Manila Bay, Philippines. Aerosol
271 sampling was also performed in a manner similar to the 2011 cruise, conducted in a series of
272 anchorages that were protected from the swell yet provided unobstructed sampling of the ocean.
273 Typically these anchorages were behind reef zones or small islands that had little breaker activity
274 or swell. Aerosol sampling was also conducted when the air was flowing within $\pm 50^\circ$ of the
275 bow on both transit and at a moorage. Given the consistent nature of winds while at moorage,
276 the *Vasco* naturally weather-vaned with the bow pointed into the wind.

277

278 While on deployment, the ship took on provisions once at Liminangcong (11.0 N, 119.3 E) near
279 the El Nido anchorage on Sept 10, and twice at Puerto Princesa, Palawan Island (9.7 N, 118.8 E)
280 overnight on Sept 13 and 19. The Puerto Princesa port calls divided the cruise into thirds, which
281 were distinct in geographic region and the sampled environment. In the first phase of the cruise
282 (Sept 4-13, 2012), the *Vasco* sampled the same locations as the 2011 cruise. From Manila Bay,
283 the *Vasco* transited to Apo Reef for a day of sampling (12.7 N, 120.5 E; Sept 6, 2012), followed
284 by a day at Coron Island (11.9 N, 120.3 E, Sept 7, 2012) and finally four days on a station at El
285 Nido behind the Guntao Islands reef (11.1 N, 119.2 E; Sept 8-12, 2012). On the 12th, the *Vasco*
286 transited the east side of Palawan Island to provision in Puerto Princesa overnight on the 13th.
287 Given the prevailing winds at the time, the second phase of the cruise brought the *Vasco* to the
288 very southern tip of the Palawan Archipelago to the western side of Balabac Island in the



289 Balabac Great Reefs (7.9N, 116.9E; Sept 15-19), 100 km north of the northern tip of Borneo.
290 This site provided excellent shelter from waves and breakers, while experiencing unobstructed
291 sampling of air from the southern South China Sea. Returning to Puerto Princesa on Sept 19 and
292 departing on Sept 20, the *Vasco* then entered its third phase of sampling; the middle of the Sulu
293 Sea at Tubbataha Reef (8.8 N, 199.9 E) at two very close moorages Sept 21-26. The *Vasco* then
294 had a final return to Navotas Manila Bay Sept 26-29, 2012.

295

296 2.3 Regional AERONET Measurements

297 The maximum extent of 7SEAS aerosol observations throughout the MC occurred during the
298 2012 Southwest Monsoon season, collinear with cruise activities. Specifically relevant to the
299 analysis of 2012 *Vasco* cruise, over fifteen AEROSOL Robotic Network sun photometers were in
300 operation, with start dates typically in mid to late July through October. Of these, eight were of
301 particular use for the *Vasco* analysis. These are, as displayed in Figure 1(b): (a) Jambi, Sumatra
302 and (b) Palangkaraya, southern Kalimantan in core biomass burning source regions of Indonesia;
303 (c) Singapore, (d) Tahir, Malay Peninsula, Malaysia, (e) Pontianak, western Kalimantan and (f)
304 Kuching, Sarawak as key coastal exit sites; and (g) Marbel University, Mindanao and (h) Nha
305 Trang, Vietnam as outer boundaries and receptors. While there are many other sites in the
306 region, they are not used here because of instrumentation failure or excessively high cloud cover.
307 To track overall smoke or pollution transport, we utilize the AERONET operational 500 nm daily
308 averaged fine-mode AOT derived from Level 2.0 Spectral Deconvolution Algorithm (SDA)
309 Version 4.1 (*O'Neill et al.*, 2003). Use of the SDA allows us to track fine-mode particles such as
310 from biomass burning or anthropogenic sources (*Kaku et al.*, 2015) while at the same time
311 removing the influence of thin cirrus contamination which can be large in this region (*Chew et*
312 *al.*, 2011).

313

314 2.4 Ancillary Model and Satellite Data

315 To capture the nature of the 2012 cruise period a number of model and satellite products were
316 used. The Navy Global Atmospheric Prediction System (NOGAPS; *Hogan and Rosmond*, 1991)
317 is used to provide baseline meteorological data for analysis as well as drive offline Navy Aerosol
318 Analysis and Prediction System (NAAPS) aerosol simulations. While NOGAPS horizontal
319 resolution is $\sim 0.5^\circ$ in this region, spectral files were truncated to $1^\circ \times 1^\circ$ for modeling aerosol



320 transport of this season in a configuration consistent with the NAAPS reanalysis (*Lynch et al.*,
321 2015; submitted). In NAAPS four species are simulated: dust, biomass burning smoke,
322 anthropogenic/biogenic fine, and sea salt. In the reanalysis configuration, smoke fluxes are
323 driven from the MODIS smoke source function drawn from a MODIS-only version of the Fire
324 Locating and Monitoring of Burning Emissions (FLAMBE; Reid et al., 2009). NAAPS
325 capability for smoke characterization in the Maritime Continent region has been demonstrated
326 (e.g., Hyer and Chew, 2010; Reid et al., 2012; 2015; Xian et al., 2013), and has been even further
327 improved upon in this reanalysis version. To account for the multitude of anthropogenic and
328 biogenic sources of fine particles, a combined anthropogenic and biogenic fine (ABF) species is
329 generated, based on a combination of Monitoring Atmospheric Composition and Climate-City
330 (MACCity) and Model of Emissions of Gases and Aerosol by Nature (MEGAN) emissions
331 inventories. Quality-assured AOT retrievals from MODIS and MISR observations are
332 assimilated into the model using a two-dimension variational (2D var) technique (*Zhang et al.*,
333 2008; Shi et al., 2011; Hyer et al., 2013). To better constrain aerosol particle wet deposition, the
334 Climate Prediction Center (CPC) MORPHing product (CMORPH, *Joyce et al.*, 2004) is used
335 instead of the native NOGAPS precipitation field for aerosol scavenging (*Xian et al.*, 2009).

336

337 For tropical cyclone information on track and intensity, we utilize the best track statistics from
338 the Automated Tropical Cyclone Forecasting (ATCF) system (Sampson and Schrader, 2000). Air
339 mass histories are also evaluated using the NOAA Hybrid Single Particle Lagrangian Integrated
340 Trajectory (HYSPLIT) Version 4.9 Model (*Draxler & Hess*, 1997, 1998; *Draxler*, 2004) based
341 on the GDAS1 $1^\circ \times 1^\circ$ global meteorological dataset. Back trajectories were typically run for 72
342 hours. These trajectories do not directly enter in the narrative here, but are presented in the
343 analysis by Atwood et al. (2016; to be submitted). It is well understood that such trajectory
344 analysis can be problematic in regions such as the Maritime Continent, with strong high frequency
345 features such as land sea breeze and orographic flows (Atwood et al., 2013; Wang et al., 2013).
346 Thus, here we only use such analyses at the qualitative level.

347

348 The *Vasco* data analysis was enhanced by using geostationary MTSAT satellite products (visible,
349 IR, cloud heights, scatterometer, etc.) as found on the NEXSAT website (*Miller et al.*, 2006;
350 <http://www.nrlmry.navy.mil/nexsat-bin/nexsat.cgi>). Regional precipitation was also monitored



351 by the aforementioned CMORPH product. MODIS active fire hotspot analysis were utilized
352 based on the similar analysis structure of Reid et al. (2012; 2015), with context as laid out in
353 Hyer et al. (2013). NASA MODIS Col 6 level 3 data were also used (Levy et al., 2013). Due to
354 the heavy cloud cover there is limited space-based CALIOP data available for smoke events over
355 the South China Sea corresponding to cruise periods.

356

357

358 3.0 RESULTS I: REGIONAL METEOROLOGICAL AND AEROSOL CHARACTERISTICS 359 OF THE 2012 BURNING SEASON

360 The 2012 *Vasco* cruise covered most of September, which corresponds to the second half of the
361 August-September high season for burning in Borneo and southern Sumatra (Reid et al., 2012).
362 This period is generally associated with strong southwesterly winds up the South China Sea
363 region and eastward progression of monsoon onset across the MC over time (Chang et al. 2005;
364 Moron et al. 2009). Smoke and pollution emissions on the islands are then transported across the
365 South China, Sulu and Celebes Seas by the prevailing monsoonal winds (Reid et al., 2012; Wang
366 et al., 2013; Xian et al., 2013). It is not necessary to go into details of smoke transport patterns
367 and their relationships to key meteorological indicators, as these are covered in the above papers
368 as well as in the 2011 *Vasco* cruise case, which fit many conceptual models quite well. However,
369 2012 did show some anomalous behavior which is worth a description here.

370 The overall NOGAPS-derived monsoonal flow, over-plotted with the CMORPH satellite
371 precipitation dataset of the core burning months, August and September 2012, is provided in
372 Figure 2, along with the MODIS Terra MOD08 average cloud cover. Corresponding information
373 on MODIS fire detections (MOD and MYD 14) and their relationship to the MJO and regional
374 TCs is provided in Figure 3. At first glance, overall flow patterns are as expected with
375 southeasterly surface winds over the South China and Sulu Seas, veering with height to near
376 westerlies at 700 hPa. South of Borneo, winds are more easterly, wrapping around the islands of
377 Borneo and Sumatra. Precipitation gradually increases from the south to the north, with a
378 maximum east of the Philippines in association with the overall monsoonal trough MODIS cloud
379 cover is spatially correlated with precipitation, ranging from over 50% in southern Borneo to
380 near 100% around Luzon. Other notable cloud and precipitation enhancements include an area
381 west of Sumatra in association with a local vorticity maximum as winds transition from easterly



382 to westerly (Wu et al., 2009; Reid et al., 2012), the Bay of Bengal in association with monsoonal
383 flow convergence onshore of Peninsular Southeast Asia, and the region west of Luzon,
384 Philippines, a result of where the monsoonal flows intersect the land (e.g., Cruz et al., 2013).
385 Regions of enhanced fire prevalence (Figure 3(a)) were consistent with the fire baseline of Reid
386 et al. (2012), and are understandably opposite of precipitation. The most typical fire hotspots of
387 Central Sumatra/Riau, Southern Sumatra/Sumatera Selatan and Southern Kalimantan provinces
388 of Borneo are clear.

389

390 Key meteorological features of concern for biomass burning in the MC include: a) the
391 interannual El Niño Southern Oscillation (ENSO), which has broad correlation to precipitation
392 anomalies and hence fire (e.g., Nichol, 1998; Field and Shen 2008; Reid et al. 2012); b) the
393 seasonal migration of the monsoon; and c) the ~45 day Madden Julian Oscillation (MJO) that
394 brings longer periods of regional convection and breaks (Zhang, 2005), which in turn has a
395 strong influence on fire emissions and aerosol lifecycle (Reid et al. 2012). Correlated with these
396 are numerous other phenomenon, including the onset and length of the monsoon season (Staub et
397 al., 2006; Cook and Buckley, 2009; Tong et al., 2009), tropical cyclone activity (e.g., Maloney
398 and Hartman, 2001), diurnal cycle of precipitation (e.g., Peatman et al., 2014) and off-island
399 airflow, which that are related to aerosol activity and transport (Reid et al., 2012; Wang et al.,
400 2013). For the 2012 southwest monsoon season, the mean Oceanic Niño Index (ONI) was
401 slightly warm, at +0.3 to +0.4°C for July through October coming out of a ~0°C neutral index in
402 the boreal spring. While in a warmer phase, the burning season is still considered neutral ENSO
403 conditions based on the commonly-used 0.5°C threshold. In comparison, the 2011 southwest
404 monsoon showed decreasing ENSO ONI index temperatures of ~-0.3°C to -0.7°C throughout the
405 season. Thus, we expect overall enhancement in 2012 burning activity. Reid et al. (2012) noted
406 that there appeared to be a correlation between positive ENSO phase and earlier monsoonal
407 transition from the Southwest to the northeast phases. In 2012, the monsoonal transition
408 appeared to be consistent with this warmer ENSO phase, with northeasterly winds returning by
409 the end of first week of October. Based on the fire count baseline of Reid et al. (2012), overall
410 burning in Central Sumatra was within ~10% of the Terra + Aqua MODIS time-series average,
411 while Southern Sumatra biomass burning was at a level about 0.5 standard deviations (~20%)
412 above the time-series average.



413

414 Overall fires in greater Indonesian and Malaysian Borneo were lower by a half to a third
415 compared to the large El Nino events of 2004, 2006, and 2009, but still ~50% higher than all
416 other negative or neutral ENSO years since combined MODIS measurements could be made
417 (2003). This is expected for a borderline high ENSO anomaly season. In comparison to the
418 2011 cruise, which had much higher burning than one would expect for a negative ENSO phase,
419 fire prevalence for the season 2012 was ~10 -20% higher than 2011.

420

421 If ENSO and the seasonal monsoon migration set the bounds of the burning season, the MJO
422 often regulates the temporal variability and transport within that period. This is demonstrated in
423 a plot of the phase and amplitude of the Wheeler and Henderson (2004) index, Figure 3(b), along
424 with seasonal fire activity in Figure 3 (c), which shows a five-day box car average time series of
425 combined Terra and Aqua MODIS fire hotspot data for June through October that are broken
426 down into the five key regimes defined in Reid et al., (2012; 2015): Central Sumatra, Southern
427 Sumatra, Indonesian Kalimantan-Borneo (an aggregate of western, southern and eastern
428 Kalimantan), Malay Borneo (Sabah and Sarawak), a combined Sulawesi, Java, and Timor
429 aggregate, and finally far-eastern Maluku and the entire island of New Guinea.

430

431 In 2012, MJO activity during the burning season was generally weak, although nevertheless
432 present. The burning season was initiated by a moderately strong MJO from May into early
433 June, with amplitudes well above 1, especially for the drier phases in the MC (phases 5-8). This
434 MJO was related to the first major burning event that emerged from Central Sumatra in June.
435 This short but dramatic pulse is a common feature in the MODIS record, and is likely the result
436 of agricultural burning, or fuels which had been stacked and ready for the first sufficiently dry
437 southwest monsoon period (Reid et al., 2012), which in this case, a strong late phase MJO event
438 provided. While much attention has been paid to the “anomalous” June 2013 burning and smoke
439 event in Sumatra which severely reduced air quality on the Malay Peninsula, this is actually a
440 recurring feature (Reid et al., 2012), although the impacts to Singapore for that year are still
441 unprecedented for June.

442



443 The next MJO cycle, while starting strong in the Indian Ocean in mid-June (Phase 1 & 2) failed
444 on approach to the MC. A weak MJO event replaced this, although it could be argued that it is
445 really the same event. As this MJO progressed to later phases, a second greater peak in August
446 burning in Central Sumatra and Western Kalimantan (apparent in a peak in the greater
447 Indonesian Kalimantan domain) appeared. From this point, the burning pattern was eastward-
448 propagating through the season, which is consistent with the eastward migration of the monsoon
449 as described by Moron et al. (2009).

450

451 The third relevant MJO cycle, which also coincided with the *Vasco* cruise, formed in the Indian
452 Ocean in mid-August, with MJO amplitudes as high as 2 through early Phase 3 (the MJO
453 entering the MC). Upon reaching the MC in the last week of August, however, the amplitude
454 weakened significantly, to less than 1 (below the significance level), and propagation was slow
455 from Phase 3 to Phase 6 (the period when the MJO is transiting the MC) and subsequently died
456 off by the end of September. Nevertheless, fire activity tracked this event, reaching a peak at the
457 end of September. This event was then followed by another weak, although complete, event in
458 October and November (not shown); not an uncommon occurrence for MJO propagation across
459 the MC (Zhang, 2005; Peatman et al., 2014). The implication for 2012 is that more significant
460 smoke generation and transport events advecting across the South China Sea would have been
461 observed had this MJO progressed in a more typical fashion. Instead, the stalling of the MJO
462 over the Maritime Continent would bring additional rainfall over the ocean (e.g., Chen and
463 Houze 1997; Peatman et al., 2014), further shortening aerosol lifecycles.

464

465 Embedded in the MJO signal is the influence of TCs. When TCs are located just west of the
466 Philippines or transiting westward into the South China Sea, two significant meteorological
467 impacts on aerosol lifecycle often occur (Reid et al., 2012). First, large scale upper-level
468 subsidence around the TC can inhibit convection and rainfall in the region, thus promoting
469 biomass burning (and enhancing its observation from space). But, simultaneously a long area of
470 monsoonal enhancement akin to an inflow “arm” often forms to the south and west of the TC,
471 leading to enhanced flow from biomass burning source regions up the South China Sea but also
472 within the monsoonal enhancement, increased convection leading to scavenging. The balance of
473 these two factors in production, advection and regional changes to precipitation allows TCs to



474 simultaneously modulate multiple aspects of aerosol lifecycle. From ATCF, the 2012 Western
475 Pacific had 25 named storms compared to 26 in the long term average. Noteworthy is that when
476 TCs were east of the Philippines (as marked in Figure 3(b)) this coincided with peaks in
477 observed biomass burning activity.

478

479 Moving from burning activity to resultant AOT, from a biomass burning perspective, the 2012
480 season showed higher burning-region AOTs in comparison to the 2011 cruise and the ENSO
481 neutral baseline provided in Reid et al. (2012). Overall core August and September burning
482 season monthly AOTs from Terra MODIS and NAAPS are provided in Figure 4(a)-(d). Because
483 of the widespread cloud cover (e.g., Figure 2(b)), both satellites and models have extreme
484 difficulty characterizing aerosol in the region (Reid et al., 2013; Sessions et al., 2015).
485 Ultimately, it is difficult to perform a pairwise analysis. Nevertheless, these products provide
486 qualitative insight into regional aerosol behavior.

487

488 In agreement with the temporal series of biomass burning in Figure 3, we see a shift from high
489 AOTs in Central Sumatra in August to more southern Sumatra and southern Kalimantan in
490 September. The highest AOTs tend to be over or near the islands. Moderately high AOTs
491 ($\sim > 0.2$) do cover the greater part of the South China Sea over the course of the entire season.
492 Differences between MODIS and NAAPS are a result of a number of causes, including sampling
493 differences (there are very few MODIS retrievals available, whereas NAAPS data is continuous),
494 and underestimates in modeled emissions due to cloud cover that limits FLAMBE efficacies.
495 Notable in the NAAPS data in particular, is that, in August (Figure 4(c)), smoke from Central
496 Sumatra propagates up across the entirety of the South China Sea, whereas in September (Figure
497 4(d), AOTs are higher in the southern South China and Celebes Sea. As discussed in Section 4,
498 this is a result of easterly waves and the influence of TC induced monsoonal enhancements and
499 inflow arms.

500

501 The best indicator for regional AOTs however is from AERONET, which can, through the SDA
502 method, minimize thin cirrus contamination (Chew et al., 2011). Included in Figure 4 are the
503 time series from AERONET sites deployed for the 2012 season, including the first AOT
504 measurements made in the heart of the burning areas on Sumatra and Kalimantan, Borneo. The



505 500 nm fine-mode AOT from key AERONET sites is also shown in Figure 4 for August through
506 October when the full network was deployed. Sites provided include: (e) Jambi, Sumatra and (f)
507 Palangkaraya, Central Kalimantan, respectively in core Sumatran and Borneo burning areas.
508 Also shown are: (g) Singapore and (h) Tahir on the Malay Peninsula and (i) Pontianak and (j)
509 Kuching on the western and northwestern coasts of Borneo, respectively. These sites provide
510 AOTs as smoke plumes leave the islands. Finally, long-range receptor sites at (k) Notre Dame of
511 Marbel University, Mindanao and l) Nha Trang, Vietnam are given. These sites are also marked
512 on Figure 4(a).

513

514 Regional fine-mode AOTs, to a certain degree, were correlated with the fire signal, but not
515 exceedingly so; perhaps due to the high coverage of cirrus clouds that can affect satellite fire
516 observations more than it affects AERONET with its SDA extraction of fine-mode AOT (*e.g.*,
517 see observability review by Reid et al., (2013)). Also, the weaker MJO periods or TCs may have
518 perturbed the transport of smoke off-island. Singapore was the only site operating for the mid-
519 June burning event; it showed slightly-elevated fine 500 nm AOTs on the order of 0.5 above the
520 background of 0.3 (not shown). For the greater August through September burning season, in the
521 source regions of Sumatra and Kalimantan, the Jambi and Palangkaraya AERONET sites showed
522 multiple events of 500 nm AOT greater than one; reaching over three at the end of the season just
523 before the monsoonal transition. As demonstrated in the comparison of the Singapore and Tahir
524 site AOTs, smoke transport off Sumatra favored the southern end of the Malay Peninsula, with
525 the exception of a large event in early August. The Pontianak and Kuching sites on the western
526 side of Borneo showed moderately high AOTs for the entire season, with 8+ events having AOTs
527 over 0.5, peaking just before the end of the monsoon. Finally the typically clean receptor
528 location of Marbel University, Mindanao showed several significant enhancements in fine-mode
529 AOT values above 0.2 in mid-September and early October. Nha Trang, Vietnam typically
530 showed background levels, with the only enhancement being by continental Asian emissions in
531 north/northwesterly flow at the end of the monsoon.

532

533 4.0 RESULTS II: THE METEOROLOGICAL AND AEROSOL ENVIRONMENT

534 MEASURED DURING THE VASCO CRUISE



535 Based on the Section 3 analysis, at first glance one would expect a nominally “typical” year for a
536 slightly-warm ENSO phase. Elevated fire activity and emissions superimposed on a near
537 climatologically average wind field should systematically yield large smoke events propagating
538 across the South China and Sulu seas in a manner very similar to the 2011 cruise as reported in
539 Reid et al. (2015). However, while the averages are close to normal, the daily meteorology
540 during the 2012 was quite variable, with two extremely weak monsoonal flow periods separated
541 by the influence of two category 5 typhoons that slowly propagated northward east of the
542 Philippines. As is presented in Section 3.3, this modulation in monsoonal strength coupled with
543 a longer cruise extent resulted in observation of much more variable aerosol behavior in 2012
544 than 2011.

545

546 *4.1 The regional meteorological environment during the Vasco cruise*

547 The overall meteorological and aerosol behavior during the 2012 cruise period is best described
548 by simultaneous examination of Figures 5 and 6. Figure 5 provides combined daily average
549 NOGAPS winds at the surface (black) and 700 hPa (magenta) overlaid with the CMORPH daily
550 average precipitation for four representative days during the cruise, marked with the *Vasco*'s
551 location. For each day, the 2:32 UTC (~9:32-10:32 LST) MTSAT false-color visible image is
552 also provided, annotated with the *Vasco* location and TCs in the area. Figure 6 then provides the
553 corresponding *Vasco* data time-series of key meteorology, including ventilated temperature, RM
554 Young wind, and disdrometer-derived precipitation. Also shown are key aerosol and gas data,
555 during appropriate sampling conditions. Included is the particle counter concentrations, PCASP
556 derived aerosol volume, and whole-air gas can-sampled carbon monoxide (CO). Finally, the
557 derived NAAPS fine-mode surface aerosol concentrations of biomass burning (gold) and
558 anthropogenic fine (red) are also provided.

559

560 The most notable aspect of the 2012 cruise relative to the 2011 counterpart, or indeed all other
561 7SEAS regional studies, was the extreme variability in the monsoonal flows. While at the
562 seasonal mean level, wind patterns seemed near normal, during the entire month of September
563 2012, daily flow patterns over the South China Sea changed measurably. These periods were
564 largely defined by the migration of two tropical cyclones (TC 17 W Sanba and TC 18 W
565 Jelawat), separated by easterly waves with significant flow reversals (e.g., Figure 5). During the



566 very first week at sea, monsoonal flow across the SCS was weak, associated with a westward
567 propagating wave consistent with the features of a tropical depression/easterly wave. The day of
568 departure (Sept 4, 2012) the Sulu Sea was already under the influence of an easterly wave, with
569 southeasterly winds at the surface and nearly calm winds through the mid troposphere. Over the
570 next two days, winds shifted with the propagation of the wave, from southeasterly, to westerly
571 and northwesterly into the eastern part of the SCS, followed by full westerly and even northerly
572 winds by Sept 7 (Figure 5 (a)). Winds at 700 hPa even became strong northeasterly. Thus for
573 the first five days of the cruise at Apo Reef, Coron, and the first several days at El Nido, sampled
574 winds were largely not from the South China Sea, but rather off of the Philippine islands of
575 Luzon, Mindoro, and Iloilo. This is evident in the *Vasco* time series where winds are generally
576 light with often a northerly or even easterly component.

577

578 Monsoonal flow and precipitation began developing on Sept 10th in association with the
579 formation of what would become super-typhoon Sanba (TC 17 W) at Palau, while the *Vasco* was
580 stationed in El Nido. By Sept 12, TC Sanba grew to typhoon strength, followed by rapid
581 intensification to category 5 the very next day. The slow northward migration of TC Sanba
582 resulted in enhanced westerly components of the marine boundary layer and mid-tropospheric
583 winds, as well as enhanced precipitation in a well-defined zonally-aligned monsoonal
584 enhancement/inflow arm. The *Vasco* transited to Puerto Princesa on Sept 12th and 13th, still
585 under significant influence of the inflow arm of TC Sanba. Upon departure from port on the
586 14th, heading for Balabac Island at the southern tip of the Palawan Archipelago, the slow moving
587 super-typhoon was still west of Luzon, with a well-defined inflow arm across the South China
588 Sea. Even through Sept 16th (Figure 5(c)), the influence of TC Sanba lingered as a inflow arm
589 extended from the Malay peninsula through Luzon.

590

591 For Sept 17th through 21st, monsoonal winds slackened yet again, with westerly winds in the
592 northern region, and even some northerly components in the lower free troposphere. This is
593 consistent with the propagation of a second easterly wave across the region. During this period
594 the *Vasco* transited back to Puerto Princesa (Sept 19th) and finally out to its last station at
595 Tubbataha Reef in the middle of the Sulu Sea. While on station there, monsoonal flow returned,
596 with the formation of another super-typhoon, Jelawat (TC 18 W). Jelawat had a similar lifecycle



597 to Sanba, forming over Palau and slowly migrating up the eastern side of the Philippines with a
598 well-defined inflow enhancement across the South China Sea (e.g., Sept 24th Figure 5(d)). Also
599 like TC Sanba, TC Jelawat intensified rapidly, becoming a category 5 super-typhoon; the
600 strongest of the season. While surface winds had a typical southwesterly direction, winds in the
601 free troposphere had significant northerly components across the South China Sea; unusual
602 relative to the more typical westerly to southwesterly winds. The *Vasco* then returned back to
603 home port in Navotas, Manila (September 27-29th) on the southern edge of the northward
604 propagating inflow of TC Jelawat. At this same time period a tropical low was forming in the
605 northern South China Sea which would eventually become tropical storm Gaemi, further
606 enhancing monsoonal flow along the Palawan Archipelago.

607

608 The meteorology described above for the 2012 cruise resulted in some marked differences from
609 the measured meteorological environment on the *Vasco* on the 2011 cruise. Perhaps the most
610 important difference was that in 2011, monsoonal flows were consistent southwesterly across the
611 South China Sea, with enhancements in low-level wind and precipitation found in inflow arms,
612 and clearer air and high aerosol loadings in regions with suppressed convection. In contrast, the
613 2012 cruise witnessed monsoonal enhancement due to tropical cyclone inflow arms, which
614 induced winds that were largely zonal in nature. The observed easterly waves also resulted in
615 much less coherent wind and precipitation patterns. Thus wind direction and speeds at the ship
616 were more variable, and precipitation occurred most days (e.g., Figure 6(b)-(d)).

617

618 Similarities between the 2011 and 2012 cruise periods were also noted. Perhaps the most
619 important was the clear presence and importance of convection and squall lines. 2012 saw an
620 increase in the frequency of convection of the South China Sea region over 2011, there was also
621 an increase in the frequency of telltale signs of cold pools, including frequent temperature drops
622 by as much as 5°C within several minutes, in combination with spikes in one-minute average
623 wind speeds to 15 m s⁻¹, and one second values as high as 25 m s⁻¹. As discussed in Section 6,
624 these cold pools also have “aerosol washout” air, dropping particle concentrations significantly.
625 Similarities and differences between these events and the cold pool events described in Reid et
626 al. (2015) will be discussed in Section 6.

627



628 *4.2 The measured aerosol environment during the Vasco cruise*

629 The far-reaching extent of the 2012 cruise, coupled with the more variable monsoon
630 meteorology, resulted in much more dynamic aerosol behavior sampled during the 2012 cruise
631 relative to 2011. In the 2011 cruise, when the *Vasco* was anchored outside of El Nido, two 2-3
632 day large-scale aerosol events with $\sim 15\text{-}30 \mu\text{g m}^{-3}$ fine-mode mass concentrations and $\text{CN} =$
633 $1000\text{-}4000 \text{ cm}^{-3}$ were sampled, separated by periods of very clean conditions ($< 1 \mu\text{g m}^{-3}$,
634 $\text{CN} < 150\text{-}300 \text{ cm}^{-3}$). The nature of aerosol events in 2012 followed similar pathologies to 2011,
635 with TCs enhancing winds and into the inflow arms. The balance between precipitation and
636 convective inhibition due to large scale subsidence from the TCs, or dry layers advected from the
637 Indian Ocean, induced these aerosol events, which were qualitatively captured by the NAAPS
638 aerosol simulations. Additional high-frequency drops in aerosol loading were also found in
639 association with cold pools; some associated with long lasting convective squall lines.

640

641 While some low frequency phenomena occurred during 2012, the 2012 cruise also showed
642 variability in aerosol events over short time scales. Inspection of the 2012 cruise time series of
643 aerosol-relevant parameters in Figure 6 shows a great deal of variability in aerosol and CO
644 loadings. For example, while there was one period of overall aerosol enhancement from
645 September 13th through the 18th, the most significant pulses (Sept 14 & 25) in inferred aerosol
646 mass concentration were generally less than 6 hours in duration; as opposed to two to three day
647 event lengths for 2011. In addition, multiple short pulses of less than 3 hours were also
648 observed.

649

650 Significant enhancements in CO as measured by the whole-air samples, as high as 200-240 ppbv,
651 were found for the most significant Sept 14 & 25 cases. Indeed, the air from the open ocean
652 exhibited a very distinct “smoky” aroma for these periods. Further, while there were more data
653 outages in 2011, owing to more variable wind direction across the bow while in transit, the *Vasco*
654 did observe several high-frequency pulses of condensation nuclei, which we are confident were
655 not due to self-sampling contamination. Of particular note were spikes in CN measured when
656 the *Vasco* was moored at Apo Reef and Coron, in air masses moving offshore of the islands of
657 Mindoro and Luzon. Also, spikes were observed entering port or in the vicinity of island cities,
658 such as September 13th and 20th while the *Vasco* was downwind of Puerto Princesa.



659

660 Also notable in 2012 was the higher baseline for “background” particle concentrations in the
661 marine boundary layer. Whereas in 2011 the background ranged from 150-500 cm⁻³, in 2012 the
662 CN concentration rarely dropped below 500 cm⁻³. Part of this difference is 2012’s closer
663 proximity to Borneo source regions along the cruise track. Further, for periods when the *Vasco*
664 was in the northern region, winds were anomalous and precipitation reduced due to the presence
665 of easterly waves. Thus, there was more sampling of Philippines islands, and regionally reduced
666 wet scavenging.

667

668 In comparison to observations, the NAAPS model simulations of aerosol loadings near the *Vasco*
669 exhibited mixed performance relative to the outstanding comparisons for 2011. For example,
670 NAAPS did simulate some aspects of aerosol transport, such as the broader aspects of the Sept
671 13-18th period. However, the model had difficulty capturing the most significant pulses, such as
672 observed spikes on September 14th and 25th. NAAPS also included other moderate events that
673 did not materialize, such as Sept 10-11, and Sept 24th and 29th. NAAPS did simulate the
674 presence of some high-frequency events, although these had notable time displacement. The use
675 of satellite precipitation to constrain scavenging processes in NAAPS improves representation of
676 variability in aerosol loadings in high emission and high convection environments, although finer
677 scale features unresolvable in a 1x1 degree transport model are clearly important.

678

679 Aerosol and gas chemistry measurements provided additional insights into aerosol properties and
680 their sources. Detailed aerosol and gas chemistry is a subject of a subsequent paper, but
681 important aspects that assist in the aerosol meteorology analysis are discussed here. As the filter
682 datasets required sampling times of one-to-two days to ensure sufficient loading, much of the
683 temporal characteristics were washed out with the background. Filter-based XRF metals also
684 had a higher noise floor and thus were inconclusive. However, the DRUM data does provide
685 elemental ratios which, in combination with the PCASP data, can provide higher resolution
686 information on elemental chemistry. The 2012 cruise included a larger number of whole-air
687 samples as compared to those sampled during the 2011 cruise.

688



689 A summary of observed aerosol chemistry is provided in Figure 7. Shown in Figure 7 (a) is
690 derived non sea-salt PM_{2.5} gravimetry from filters, with corresponding quartz filter analyses of
691 organic and black carbon. For comparison, an inferred 30 minute PCASP-derived dry mass
692 concentration using an assumed density of 1.4 g cm⁻³ is presented. This value of density
693 provided good closure (unity slope; r²=0.8) between the temporally-integrated PCASP and
694 gravimetric values, and is close to the density for dry biomass burning of 1.35 g cm⁻³ as
695 measured by Reid et al. (1998). Zero values of filter mass are associated with no-sampling
696 periods due to the relative wind direction over the bow. Shown in Figure 6(b) are the Teflon
697 filter-derived K and SO₄ values, followed by 6(d) elemental ratios of vanadium and potassium to
698 sulfur from the DRUM sampler used as an indicator to separate aerosol industrial and biomass
699 burning origin. Also provided in Figure 7 are key whole-air gas sample species. While there are
700 no unique chemical identifiers to isolate natural, biomass burning and other anthropogenic
701 sources, several species warrant attention. Included are: 6(d) CO and CH₄; 6(e) benzene and
702 methyl-iodide as commonly used key indicators for biomass burning (Akagi et al., 2011); 6(f) i-
703 and n-pentane as well as their ratios, with enhanced ratios suggesting more industrial rather than
704 biomass burning sources (McGaughey et al., 2004; Simpson et al., 2014); and finally, 6(g)
705 isoprene and 2-BuONO, a photo-oxidation product of butane and indicator of photochemistry.

706

707 Figure 7 illustrates several notable aspects of atmospheric chemistry in this region. For example,
708 organic mass fractions vary significantly between the aerosol events. For the largest smoke
709 event on Sept 14th, the vanadium-to-sulfur ratio is extremely low, while the potassium-to-sulfur
710 ratio was higher, suggesting this air mass was dominated by biomass burning. The organic and
711 black carbon mass fractions were ~50% and 5%, respectively; these values are very reasonable
712 for biomass burning (Reid et al., 2005; Akagi et al., 2011). This also suggests also that the bulk
713 of the sulfate here is indeed a result of biomass burning emissions; perhaps secondary in origin
714 from primary SO₂ emissions of peat burning (Reid et al., 2013). However, there are significant
715 reductions in OC and BC for the later burning events, on the order of 25% and 2.5% for organic
716 and black carbon, respectively, and simultaneously vanadium was enhanced. The difference was
717 made up through sulfur/sulfate enhancements, ranging from 20% for the 14th event, to 30-40%
718 for the others. The sulfate-to-organic carbon ratio then increases from 0.45 for the 14th, to 1.4-
719 1.8 for the subsequent filters. Clearly, these major events had significantly different inorganic



720 mass fractions, and perhaps enhancement for MC industrial emissions. In all cases, potassium
721 was at 1.5-2% from the filters, although the potassium to sulfur ratio from the DRUM sampler
722 did show potassium enhancements consistent with increased biomass burning. All of these
723 findings as well as those from the 2011 cruise point out that “pure” biomass burning plumes are
724 relatively rare. The bulk of the polluted air mass is more often a combination of biomass burning
725 and other anthropogenic emissions.

726

727 Periods of pure pollution were also observed in the early days of the cruise. When *Vasco* was
728 under the influence of flow from the Mindoro and Luzon Islands, organic carbon mass fractions
729 were higher, at 60-to-80%, and there were very high vanadium to sulfur ratio values (~0.1). In
730 one case, Sept 11, derived OC was higher than gravimetric mass. In this case, the gravimetry
731 matched the PCASP; a sure sign that this is organic artifact. But this nevertheless suggests
732 perhaps a change in aerosol organic chemistry associated with regional anthropogenic emission.
733 Indeed in the first period, sulfate-to-organic carbon ratios were low, on the order of 0.4-0.6.
734 Potassium was particularly enhanced with vanadium against sulfate from Sept 6th. However, this
735 was a very dry period in the mission, and perhaps un-oxidized SO₂ was prevalent in the
736 atmosphere.

737

738 Gas chemistry can further help distinguish biomass burning from anthropogenic industrial
739 emissions. From a gas chemistry point-of-view, indeed the largest aerosol mass events are
740 associated with CO and consistent with biomass burning (Figure 7(d)). However, the
741 correlations between other gas species were highly variable. For example, correlations between
742 benzene and CO as commonly used biomass burning indicators are quite good (slope 0.0008 and
743 $r^2=0.72$) with the exception of an isolated spike at ~0Z Sep 20 while entering Puerto Princesa.
744 Methyl iodine, sometimes used as a burning tracer, showed numerous spikes over an order of
745 magnitude above the nominal baseline for CO and benzene (Figure 6(e)). Indeed, at times very
746 high spikes of CH₃I are present with little increase of CO. This may reflect other potential
747 sources of CH₃I such as coastal macrophytic algae (Moore and Zafiriou, 1994); not
748 unreasonable in the highly-productive waters of SE Asia.

749



750 For separation of burning emissions from non-burning anthropogenic emissions, we can look to
751 information in the concentration of i- and n-pentane and their ratio (Figure 6(f)). When the
752 *Vasco* entered or exited Puerto Princesa's urban plume, values of i-pentane increased markedly,
753 along with the ratio of i- to n- isomers, thus providing a good indicator of local city or village
754 sources. Outside of these areas, or in background conditions, n-pentane was enhanced. The
755 significant variability in i- to n-pentane demonstrates the significant variability in sources in the
756 region.

757

758 From a photochemistry point of view, spikes in isoprene were frequently found in the vicinity of
759 islands (Figure 6(g)), but also occasionally a day's distance from shore. At concentrations near
760 100 pptv, these levels are rather low compare to terrestrial source regions, where values on the
761 order of 1-5 ppbv are expected and measured (e.g., Wiedenmyer et al., 2005; Hu et al., 2015).
762 However, spot cans on the interior of islands taken as part of the 2011 *Vasco* cruise did reach 1
763 ppbv (Reid et al., 2015). Similarly, 2-BuONO₂, an indicator of photochemistry, also showed
764 sporadic behavior, in this case associated with both smoke events and urban plumes alike.
765 Finally we observed sporadic cases of strongly enhanced methane, which in general did not
766 correlate with CO or any other species. This very easily could be indicative of gas hydrate
767 derived methane production in under-ocean cold seeps in the South China Sea (*Suess*, 2014).

768

769 5.0 RESULTS: AEROSOL METEOROLOGY OF SIGNIFICANT AEROSOL EVENTS

770 From Section 4, the measured aerosol and meteorological environment during the 2012 cruise
771 was found to be much more complex than the 2011 counterpart was. The meteorology was more
772 variable, and additional aerosol phenomenon such as from urban plumes and nucleation events,
773 were sampled. Ultimately, the aerosol events were relatively short lived compared to 2011.
774 Indeed, more prevalent high frequency phenomenon, such as particle concentration drops due to
775 cold pool or the occasional spike in CN are also observable (Figure 7). In this section, we delve
776 into more detail on the aerosol meteorology of key aerosol events. To help inter-compare aerosol
777 events, particle concentrations and key whole-air can samples with associated aerosol particle
778 concentrations are provided in Table 1. Thermodynamic data for soundings collected in three
779 key events are given in Figure 8. Atwood et al., (2016; to be submitted) go into much greater
780 detail on the implications of these events to aerosol microphysics.



781

782 *5.1 Biomass Burning Events*

783 One can interpret the PCASP-inferred mass, aerosol elemental ratios, and CO versus the ratio of
784 *i-to-n*-pentane as indicative of two very clear biomass burning-dominated event periods sampled
785 on the *Vasco*: Sept 14-17th and 26th. There are also multiple small aerosol and CO
786 enhancements visible, especially late in the cruise. While we say these are biomass burning
787 events, we must emphasize that it is likely that other species were transported with the open
788 burning emissions, including urban and shipping fossil fuel emissions and biofuel. Regardless,
789 the two major event periods have every indication of being dominated by open burning
790 (including the smoke we could smell near the ship) and warrant special attention, as they give
791 key insight into aerosol lifecycle in the South China and Sulu Seas.

792

793 *5.1.1 Puerto Princesa to Balabac Sampling: The Sept 14th-17th event*

794 Details of the Sept 14th - 17th event are provided in Figure 9 for the time period from the *Vasco*
795 leaving Puerto Princesa through its Balabac anchorage and start of its return home. To describe
796 the lead up of the event, included are MTSAT visible satellite images for Sept (a) 13th and (b)
797 14th at 4:32 Z with the combined Terra and Aqua 550 nm AOT for that day. Also recall that
798 wind, precipitation, and satellite imagery for the middle of the event are presented in Figure 5(c).
799 Included in Figure 9 is the *Vasco* time series of several key parameters, including (c) PCASP
800 volume distributions, (d) temperature, (e) wind speed, and (f) precipitation. In terms of duration,
801 and of fine particle and (based on Figure 7) CO concentrations, the Sept 14-16th event was the
802 most significant burning event sampled during the 2012 cruise. Peak values for particle number
803 and CO concentration reached as high as 2000 cm⁻³ and 250 ppbv respectively, just as the *Vasco*
804 moved south from Puerto Princesa. Whole-air sample data taken at this point give all of the key
805 VOC markers of biomass burning dominated aerosol loading, including very high ethene and
806 benzene. The ratio of *i-to-n*-pentane was ~1.3, also suggesting biomass burning over other
807 anthropogenic emissions.

808

809 Based on the spike in AERONET AOT at Marbel University, Mindanao (Figure 4 (k)), this
810 smoke event extended through the Philippines into the Pacific Ocean with a fine-mode AOT of
811 0.34. Particle size distributions were fairly constant, with a dry volume median diameter of ~0.3



812 μm . While the transported smoke into the region was immediately noticed upon departure from
813 Puerto Princesa ~ 0 Z on the 14th, based on NAAPS data, it is quite possible that the event began
814 to arrive just after the *Vasco* entered the harbor for resupply 18 hours earlier. No doubt, we also
815 measured Puerto Princesa influence in the hour entering and hour leaving the harbor. However,
816 the particle and CO concentrations continued to increase as the *Vasco* transited to the south
817 toward Balabac Island, well away from any local sources. At 12 Z on the 14th, a very rapid drop
818 in particle concentrations occurred while the *Vasco* was approaching the southern tip of Palawan
819 Island (down to 500 cm^{-3}), with partial particle and CO recovery when the *Vasco* made anchor at
820 Balabac Island. There, higher particle concentrations remained for another two days with a slow
821 decay to cleaner conditions of 500 cm^{-3} , bringing the event to a close. A final peak was observed
822 and modeled in NAAPS as the *Vasco* departed for a return to Puerto Princesa near 23Z on the
823 19th.

824

825 For the transit south to Balabac, weather was relatively stormy, with moderately high winds and
826 periods of rain. On anchorage, isolated cells of precipitation were frequently observed in the
827 vicinity. The first radiosonde released occurred on the arrival at Balabac Anchorage on Sept. 15,
828 and showed generally moist conditions in the lower free troposphere. However, air was dry in
829 the upper troposphere, perhaps due to large scale subsidence in association with TC Sanba. This
830 dry air aloft may have inhibited some of the deep convection, thus allowing the transport event to
831 persist.

832

833 The Sept 14-17th event has several interesting characteristics. First, while the NAAPS model
834 generally predicted this event, the initial peak concentration was significantly underestimated.
835 Second, the dramatic drop in particle concentration ~ 12 hours into the event would normally
836 imply a cold pool. However, the particle decline occurred over a period of 45 minutes as
837 opposed to the minute or two which one would expect from a cold pool event. While there was a
838 temperature drop associated with the particle reduction, it was not as dramatic or rapid as some
839 other events. Indeed, there are actually several significant temperature drops in the hours during
840 the high concentration period with only moderate perturbations to the PCASP and CN data. The
841 NAAPS model is somehow, however, picking up on the particle concentrations in the recovery.
842 Clearly, this is not a typical cold pool event as was demonstrated in the 2011 cruise. Third and



843 finally, on the last day on station in Balabac Island, the cleanest periods of the cruise were
844 sampled. While part of this observation may be attributable to the rainfall observed at the *Vasco*,
845 the lowest concentrations were between rain events. Given the location of this ship right off of
846 the northwest tip of Borneo, higher particle concentrations were expected.

847

848 We hypothesize that the dynamics of this particular event are based on two meteorological
849 components coupled with an orography effect from Palawan Island. The first is related to coastal
850 and orographic flows in western Borneo. The September 14-16th event was initiated with a large
851 biomass burning outflow event on September 13 (e.g., AERONET data at Kuching in Figure 4(j)
852 and Figure 9(a)). Fine-mode AOTs at Kuching peaked at 1 on this date, while AOTs at
853 Pontianak, further south were constant at ~1. In the absence of significant burning in the vicinity
854 of Kuching, smoke must be transported from western and central Kalimantan regions.
855 Throughout the mission however, as seen in the model data in Figure 5, the NOGAPS model had
856 very low surface wind speeds right offshore of Kuching. In the lower free troposphere where
857 winds are higher, they tended to be westerly, thus preventing smoke above the boundary layer
858 from being advected offshore into the South China Sea. Thus in the model, the smoke does not
859 get advected offshore nearly as far as it should and smoke clings to the coast. However based on
860 MODIS AOT in Figure 9(a), we see that in fact the smoke was transported hundreds of
861 kilometers offshore. This plume feature may also have contributions from Sumatra, also
862 unresolved in the global model. As hypothesized in Reid (2012), and then demonstrated in
863 mesoscale simulations by Wang et al., (2013), the sea/land breeze and orography play a
864 significant role in modulating smoke transport on and off the islands of the Maritime Continent.
865 We hypothesize that orography and land breezes coupled with additional enhancement in
866 monsoonal flows due to TC Sanba resulted in this significant ejection event. This
867 phenomenology resulted in the significant smoke loadings at the *Vasco* as it left Puerto Princessa
868 and simultaneously missed in the model. As the *Vasco* moved south, the model was able to
869 account for the smoke that was transported closer to the Borneo coast.

870

871 The second significant feature of the Sept 14-17th event, the precipitous drop in smoke particle
872 concentrations on September 14 at 1230Z, was due to the remnant of a massive squall line,
873 clearly visible in the Figure 9(b) satellite image. Based on inspection of the MTSAT data, this



874 was formed from a series of isolated cells aligned from south of the southern tip of Vietnam to
875 the Malay Peninsula the night before. Cold pools from these cells were advected to the west as
876 part of accelerated winds over the South China Sea in association with TC Sanba, eventually
877 resulting in a clear squall line that was nearly 700 km long before daybreak on the 14th. MTSAT
878 imagery suggests the arrival of this squall line at Palawan Island at ~12Z on the 14th, coincident
879 with the drop in particle concentration. Since the wind speed of the steering flow aloft is greater
880 than that of the smoke-laden marine boundary layer air, the squall line created a large patch of
881 clean air at the surface. We also hypothesize that Palawan Island broke up this particular squall
882 line and its associated cold pool, thus slowing the more typical rapid temperature and particle
883 drop.

884

885 The third interesting aspect of the September 14-17th event is the relatively clean conditions
886 experienced at its end on September 17th. This was partially seen in the NAAPS model, but the
887 model nevertheless over predicted mass concentrations in what was the cleanest air sampled
888 during the mission, even though the *Vasco* was very close to Borneo. We believe this situation
889 was a result of the northern propagation of TC Sanba during the event. By September 15, the
890 TC's inflow arm was in the middle of the South China Sea. Surface winds along the northwest
891 Borneo coast slackened considerably, even taking on a northerly component by late on the 16th.
892 At this same time, coastal convection began to increase. By the 17th, surface and lower free
893 tropospheric winds at the *Vasco* were coming from the Central China Sea, allowing for more
894 clean conditions to be sampled. NAAPS resolved a very strong gradient in particle concentration
895 right at the *Vasco* anchorage. At 1x1 degree resolution, even a single grid-box difference made a
896 significant difference in predicted values.

897

898 5.1.2 Puerto Princesa to Tubbataha Sampling and the Sept 25th-26th event

899 The second largest biomass burning event was identified in association with the final stage of the
900 cruise while moored at Tubbataha Reef. The *Vasco* departed from Puerto Princesa to Tubbataha
901 Reef in the Sulu Sea on September 21st, and ended its sampling with the return voyage back to
902 Manila on Sept 27th. While there were sporadic peaks in particle and CO concentration on Sept
903 23rd and 24th, the event was sampled for a 12 hour period over Sept 25th-26th. This event had
904 peak particle concentrations and CO values nearly as high as the September 14-17 event, but was



905 considerably shorter in duration-nominally only eight hours long. There were also a number of
906 minor events flanking either side of the primary event. NAAPS also suggested a peak in smoke
907 concentrations, but the model predicted peak concentration 12-18 hours earlier than observed,
908 and over predicted smoke and pollution thereafter.

909

910 More detailed data from the Sept 25-27 period is presented in Figure 10 in a manner similar to
911 Figure 9. Some aspects of the Sept 25th-26th event mimic the earlier Sept 14-16th event. Particle
912 size distributions, with a volume median diameter of ~0.3 μm , were similar. Key VOC markers,
913 as listed in Table 1, looked similar to the Sept 14th event. A TC (here Jelawat) was just east of
914 the Philippines, with an extensive inflow arm reaching to Southern Vietnam (e.g., Sept 24th
915 meteorology and imagery in Figure 5(d)). A day later, as TC Jelawat migrated northward, a large
916 aerosol ejection event occurred along northwestern Borneo into the South China Sea, in this case
917 visible in both the Kuching and Pontianak AERONET time series. At the same time, NAAPS
918 and MODIS AOT data suggest that for this case, a large event also departed Sumatra, which we
919 speculate may have also been part of the sampled airmass of the principle event or perhaps the
920 secondary event that appeared 12Z on the 26th. Regardless, neither the modeling nor the remote
921 sensing data provide enough information to confidently make this attribution. Also like the
922 previous Sept 14-16th event, the TC's continued northward migration also ended the event.
923 Soundings were similar between the two events, being relatively moist in the lower troposphere,
924 with some drying aloft. Further, CMORPH data suggested development of coastal convection
925 early on the 26th.which also likely resulted in additional particle scavenging.

926

927 The comparison of the weather and PCASP time series for this event does show some interesting
928 features. Most notably, the most significant increase in particle concentration at 18Z on the 25th
929 was heralded by a cold pool with near instantaneous temperature drop and increased wind
930 speeds. Generally, we think of cold pools being associated with convectively washed-out air.
931 But in this case, particle concentrations increased, and the magnitude of the temperature, wind
932 and precipitation perturbations were quite small. Thus, the event may have been associated with
933 some minor convection along the leading edge of the airmass. But the observation does
934 nevertheless pose a question regarding a generalized view of clean air behind cold pools and
935 squall lines. Indeed, while a focus of the Sept 14th case was in the clean air behind the squall



936 line, at 6 hours before that event there were multiple temperature drops with corresponding peaks
937 in winds and precipitation, but little effect on particle concentration. These too may be indicative
938 of cold pool remnants. It is possible that the convection causing the cold pool had dissipated
939 leaving the propagating density current. As this feature moved, it may have entrained air with
940 higher particle counts. Such events may be consistent with land breeze induced coastal
941 convection.

942

943

944 5.2 Local aerosol events

945 While the primary focus of the 2012 Vasco cruise was to observe the nature of long-range
946 biomass burning and anthropogenic aerosol transport from Borneo and Sumatra to the
947 Philippines, we were mindful of the potential impact of local aerosol sources. During the cruise,
948 two significant types of local sources were observed; a nucleation event at Apo Reef on Sept. 5th
949 -6th, and a series of urban plumes as the *Vasco* neared the vicinity of port towns such as Coron
950 and Puerto Princesa. These events are discussed in more detail below.

951

952 5.2.1 Apo Reef Nucleation Event

953 The first anchorage reached after departing Manila was at Apo Reef in the middle of the Mindoro
954 Strait, on September 5th and 6th. As noted in Section 4, during this period the South China Sea
955 was experiencing strong break in the southwest monsoon. The atmosphere was relatively dry
956 above 700 hPa (Figure 8), with only scattered cumulus and congestus in the region. Boundary
957 layer and lower free-tropospheric winds were generally northwesterly to easterly in the northern
958 Philippines on these days, instead of the much more typical southwesterly monsoonal flow.
959 Consequently, sampled air masses on the *Vasco* were downwind from Luzon and/or Mindoro.
960 On September 6th at ~1Z (~9:00 AM local) the *Vasco* sampled a significant spike in condensation
961 nuclei, in excess of 1500 cm⁻³. At the same time, filter and PCASP-inferred particle mass
962 concentrations were low, only perhaps 1-3 µg m⁻³, and CO was only slightly above background
963 at ~100-110 ppbv. During this early period in the cruise, the SMPS was still operational and
964 resolved the aerosol particle size dynamics from 0.02-0.5 µm (Figure 11). Three whole-air
965 samples were also collected during the event, including 22:20Z Sept. 5th, as a pre event can,
966 2:45Z Sept 6th in the middle of the event, and 7:30Z Sept 6, for post event sample (Table 1).



967

968 The aerosol dynamics for Apo Reef show the characteristics of a classic nucleation event (e.g.,
969 see review by Kulmala et al., 2004). Leading up to the event, particle concentrations were at
970 $\sim 500 \text{ cm}^{-3}$, with an estimated mass concentration $< 1 \mu\text{g m}^{-3}$. The fine-mode particle number
971 distribution was fixed to a count median diameter of $0.1 \mu\text{m}$, but with significant enhancements
972 throughout the event. Clearly, an airmass change occurred at $\sim 23:00\text{Z}$ Sept 5, with a dramatic
973 increase in particle concentration to 1000 cm^{-3} , and a slight fine-mode particle volume increase
974 to $\sim 1.5 \mu\text{g m}^{-3}$. Nucleation was indicated at Sept 6 1Z, or nominally 9:00 local time, as solar
975 radiation was increasing throughout the morning. Total concentration peaked at 1800 cm^{-3} . The
976 count median diameter of the ultrafine mode initialized at $0.02 \mu\text{m}$, growing to $0.05 \mu\text{m}$ in five
977 hours. By 6:00Z (14:00 LST), the bimodal nature of the fine-mode aerosol population ended,
978 with a strong $0.1 \mu\text{m}$ number mode in place. The fine mass concentration was estimated to be \sim
979 $3\text{-}5 \mu\text{g m}^{-3}$ throughout the core of the event. While the ultrafine mode may have grown into this
980 fine mode, there were additional modal shifts to $0.08 \mu\text{m}$ over the next two hours, which may
981 actually be more representative of the airmass. Also noteworthy is that at $\sim 3:00\text{Z}$ a simultaneous
982 enhancement in both the fine and ultrafine mode occurred, suggesting a covariance in both the
983 fine mode particles and the nucleation event precursor gases. Indeed, this is consistent as the
984 nucleation event occurred along with a strong increase in fine particle concentration.

985

986 While a separate paper will be devoted to the whole-air samples from the 2011 and 2012 cruises,
987 it is noteworthy here that the VOC profile during the event is consistent with the nucleation
988 event, coinciding with reactive anthropogenic gas emissions (Table 1). During the event there
989 are significant enhancements in reactive alkanes, notably roughly a factor of two enhancements
990 in ethene and propene. Also notable were a factor of 2.5 increase in dimethyl sulfide over
991 background, and a slight increase in CH_4 , *i*-pentane and *i*-PrONO₂ and a decrease in CH_3I . All
992 other species were relatively constant. Interesting, isoprene was near detectable limits, as were
993 pinenes, as were pinenes, suggesting that terrestrial biogenic influences had been
994 photochemically removed upwind. Also missing are enhancements in biomass burning markers.
995 CO was fairly constant at 95-100 ppbv, as was benzene. Further the ratio of *i*- to *n*-pentane
996 increased from 1.3 to 1.7. All of this data then points to the likelihood that the nucleation
997 precursors were anthropogenic in origin from Luzon and/or Mindanao.



998

999 5.2.2 Puerto Princesa Plumes

1000 A second class of observed local aerosol phenomena was in association with urban plumes.
1001 While the *Vasco* cruise track was purposely away from population centers, there were times
1002 during transit that the influences of population centers were considerable. These ranged from
1003 small boat activity and emissions around coastal villages, to observation of the urban plume of
1004 Puerto Princesa as the *Vasco* entered and exited to take on supplies. Focusing on Puerto
1005 Princesa, the *Vasco* visited on ~Sept 13 and 20th, leading to four sets of observations. On three of
1006 these occasions, significant enhancement in particles due to the Puerto Princesa plume were
1007 clearly observed (for the exit on Sept 14, the local aerosol environment was dominated by the
1008 Borneo smoke event).

1009

1010 As the *Vasco* was nearing Puerto Princesa on September 13th, 2:00Z UTC (~10:00 LST) at
1011 approximately 30 km out, CN concentrations rapidly increased to instrument saturation at 10,000
1012 cm⁻³. At this point, the crew immediately suspected self-sampling, and quickly shut
1013 instrumentation down. However, it was then realized that the wind was in fact traveling directly
1014 over the bow. Some of the instrumentation was then restarted, and a whole-air sample was
1015 collected. While the boundary layer was clearly biomass burning-dominated upon departure the
1016 following day, the crew was prepared for sampling the plume the next visit Sept 19-20. In this
1017 case, concentrations peaked at only ~2200 cm⁻³.

1018

1019 The pair of visits, while relatively isolated samples, nevertheless provide some insight into the
1020 nature of particle populations within the Philippines Islands. Key particle and gas measurements
1021 are included in Table 1, and can be compared to the Apo Reef and biomass burning events. Most
1022 importantly, the very high particle concentrations for arrival on Sept 13 have every indication of
1023 being a nucleation event. Unfortunately, as the SMPS was inoperative for this portion of the
1024 cruise, we cannot directly compare size distributions with the Apo reef case. But comparison of
1025 PCASP and CN count showed a substantial aerosol population with diameters less than 0.1 μm.
1026 Winds were clearly in an outflow region for the city, and solar radiation was fairly intense in the
1027 late morning under only moderately cloud free skies. On the subsequent visit on September 19, a
1028 sample was taken just before arrival, and a subsequent sample was collected as the *Vasco* entered



1029 the harbor. Clear enhancements in particle concentrations were observed. Although, as reported
1030 by Atwood et al. (2016; to be submitted), there was no nucleation mode in this case, suggesting
1031 these particles were primary; this is not unexpected given the earlier time of arrival (~8:00 AM
1032 LST) and full cloud cover. Similarly, upon departure in the 21st, at 6:00 AM LST, particle
1033 concentrations were low ($<400\text{ cm}^{-3}$), even before the morning commute.

1034

1035 Whole-air sample data for these cases provide us with other useful information. First, and most
1036 notably, the use of the ratio of *i*-to-*n*-Pentane in previous studies seemed to be justified, with
1037 values above 2 being clearly associated with the urban plume, and also slightly enhanced in the
1038 Apo Reef plume. Also hexane, a gasoline derivative, also appears to be a strong signature for
1039 Puerto Princesa. But in general, for most species, the differentiation between “urban” and
1040 “biomass burning” in older plumes is not so straightforward.

1041

1042 6.0 DISCUSSION: COMPARISON OF THE 2011 AND 2012 STUDIES

1043 This paper had three primary objectives: 1) provide a broad overview of the 2012 *Vasco* cruise,
1044 including instruments carried, cruise track, and the general characteristics of the regional
1045 environment sampled; 2) apply the 2012 *Vasco* as a vehicle for continuing the narrative put forth
1046 in the 2011 effort on the nature of aerosol populations associated with the southwest monsoon,
1047 thus bridging climatological indicators commonly used to assess aerosol lifecycle to real world
1048 meteorology; and 3) relate how aerosol properties co-varied with regional meteorological
1049 phenomenon in order to establish the extent to which biomass burning or industrial pollution
1050 from the southern Maritime Continent can be transported towards or into the boreal summer
1051 southwest monsoonal trough. To our knowledge, these cruises provide the first published
1052 aerosol field measurements in the boreal summertime South China and Sulu Sea regions.

1053

1054 The similarities and contrasts between the 2011 and 2012 burning seasons and cruise
1055 observations portray key aspects of the southwest monsoon aerosol system, pointing to a number
1056 of pressing observational and prediction challenges. Certainly from an inter-seasonal, seasonal,
1057 and even monthly time period, the conceptual models of aerosol lifecycle in the southwest
1058 monsoon of Reid et al. (2012) largely holds. At an inter-seasonal scale, ENSO phase is related to
1059 precipitation deficits and hence more burning in the MC. This ENSO cycle also effects monsoon



1060 onset and transition. Within the season, the MJO, in part, regulates large-scale precipitation
1061 patterns, which then affects event timing. Tropical cyclones develop well-defined areas of
1062 monsoonal enhancement/inflow arms with accelerated surface winds that help draw smoke
1063 further into the monsoonal flow, and but may also lead to enhanced scavenging. Major land/sea
1064 breeze events can lead to significant aerosol ejection off island. Ultimately, multi-day events are
1065 possible, such as the two events for 2011, and the Sept 14-17 event for 2012. Finally, while near
1066 “pure” biomass burning events are possible, there is more typically a mixture of biomass burning
1067 and other anthropogenic emissions. Both the comparison of the seasonal behavior and the
1068 measurements on the cruises bear these similarities out.

1069 Several key differences between long-range transport characteristics in 2011 and 2012 are highly
1070 noteworthy. First, while the monsoon frequently has weak and strong phases, the 2012 case
1071 clearly showed how strong the effect of tropical waves moving through the region can be on low-
1072 level flow patterns. Indeed, the first week of the 2012 cruise coincided with uncommonly clear
1073 skies and even northerly winds. Such clear areas provide some of the rare opportunities for
1074 satellite observations. Yet from a climatological point of view provide, this clear sky bias
1075 fundamentally represents a skewed portrait of the aerosol system (Reid et al., 2013). Additional
1076 studies are already underway to ascertain the specific representativeness of aerosol particles in
1077 the region.

1078 A second significant difference between 2011 and 2012 is that while a multi-day event occurred,
1079 many shorter events were observed in the latter year. This is likely in part due to the closer
1080 proximity of the *Vasco* to Borneo, and we speculate that a more significant role of convection
1081 along the coast of Borneo led to more pockets of smoke. Further in 2012, the *Vasco* did not
1082 experience a regional severe clear day as there was at the end of the 2011 cruise that was caused
1083 by a TC propagating across Luzon and into the South China Sea. This then leads to suspicion
1084 that many pockets of polluted air can be migrating through the region, in between convective
1085 cells but still obscured from satellite detection, on a regular basis.

1086 High-frequency events in 2012 also included observation of two nucleation events and urban
1087 plumes. While it is often thought that these types of nucleation events only occur in the presence
1088 of gas precursors but few aerosol particles (e.g., Mäkelä et al., 1997; Kulmala et al., 2004; Boy et
1089 al., 2008), for the tropics and subtropics, nucleation events have also been noted in polluted



1090 urban environments (e.g., Cheung et al., 2011; Betha et al., 2013; Kanawade et al., 2014, Brines
1091 et al., 2015) and even dense tropical smoke plumes (Reid et al., 2005). The *Vasco* observed both
1092 kinds. The Apo reef nucleation event seemed to follow the more traditional relationship, with
1093 precursor gases in the presence of low aerosol particle surface area. Indeed, while in clean mid-
1094 latitude marine conditions, Covert et al., (1992) observed explosive nucleation events and
1095 discounted local or transported sources. Instead, they suggested such an event being a natural
1096 outcome for a marine boundary layer having low particle surface area. This later argued that
1097 nucleation in some of these remote sub-tropical to mid latitude areas are assisted by ion-mediated
1098 nucleation events (IMEs) formed by the ionization of molecules by cosmic rays (Yu et al.,
1099 2008). While Yu et al., (2008) considers such nucleation generally unfavorable in tropical
1100 regimes and the interior of the MC, they did predict significant nucleation on the periphery-
1101 notably west of the northern Philippines, south of Java and east of New Guinea. Indeed, Yu et al.,
1102 (2018) placed a nucleation hotspot right at our point of observation. Aided by anomalously clear
1103 skies, and thus likely high photolysis rates we see this nucleation mechanism as being reasonable
1104 contributor to the event. Indeed, it was the only such observed event in the two *Vasco* cruises.

1105 For the *Vasco* case, we indeed had low particle concentrations, but we must consider
1106 enhancements due to the presence of reactive VOCs. Indeed, parts of Luzon are heavily
1107 populated, such as Manila, and there are many other urban centers, such as Batangas, ~200 km
1108 northwest of where we were anchored. In between are countless small villages, large shipping,
1109 and small fishing boat activity, all of which are capable of producing photochemical precursors
1110 and hence promoting nucleation events such as those observed. Thus, while particle mass
1111 concentrations (and hence AOT) may be low, there are likely many pockets of high CCN
1112 concentration generated from remote islands.

1113 The second type of nucleation event, in the outflow of a polluted urban plume, was also observed
1114 by the *Vasco* outside of Puerto Princesa. Nucleation events with concentrations this high have
1115 been reported in urban tropical air in late morning (e.g., Cheung et al., 2011; Betha et al., 2013;
1116 Kanawade et al., 2014, Brines et al., 2015). For Singapore, enhancements of higher than
1117 10,000+ cm⁻³ were frequently observed, dramatically shifting the size distribution to smaller
1118 sizes (Betha et al., 2013). Ultimately, whether in clean or more polluted conditions, aerosol
1119 nucleation events are probably not uncommon in the Maritime Continent.



1120 In addition to nucleation events, the *Vasco* in 2012 intersected many small plumes, as well as the
1121 strong urban plume of Puerto Princesa (population \approx 250,000). These observations remind us
1122 that while many of the islands of the MC are thought of as “remote”, outside of the megacities,
1123 they can nevertheless harbor reasonably sized populations. Given the significant use of biofuel
1124 or highly polluted engines, these islands can clearly emit significant amounts of CCN. The
1125 relationship between these nucleation events and urban plumes to CCN dynamics is discussed at
1126 length in Atwood et al., (2016; to be submitted).

1127 Finally, and perhaps most interestingly, the 2012 cruise demonstrated a new relationship between
1128 aerosol events and convective cells and more organized squall lines. In 2011, drops in particle
1129 concentration were coincident with temperature; consistent with the notion that cold pool air was
1130 advecting into the region with aerosol particles already deposited out. As the profiles show wind
1131 shear and variable wind speeds, the steering winds of the squall lines roll over polluted airmasses
1132 underneath. Thus, these squall lines could be likened to “lawn mowers” ingesting or scavenging
1133 aerosol particles as they propagate.

1134 Based on the work of Seigel and van den Heever (2012), which showed that dust generated
1135 ahead of cold pools on the leading edge of thunderstorms is lifted to mid-levels where the
1136 potential impact of aerosol particles as CCN was minimal, the 2011 cruise suggested that the
1137 nature of convection in the region often insulated itself from potential aerosol impacts.
1138 Certainly, the *Vasco* observed some of this behavior in 2012, but also observed the opposite;
1139 cases where the telltale cold pool signs of rapid temperature drop and spikes in wind heralded the
1140 coming of a polluted airmass. Indeed, during the 14th-18th September period in Figure 9, both
1141 clear air and polluted air followed cold pools. While the wiring diagram for larger scale features
1142 is largely well known, and to some extent can be qualitatively captured by a coarse-grid model
1143 such as NAAPS with additional constraint from satellite precipitation products, there remains
1144 much to understand about aerosol lifecycle in the vicinity of convective cells and squall lines.
1145 We suspect that a clue to the behavior where air pollution is following cold pool event lies in the
1146 rather shallow temperature drops (1-2°C versus 5-6°C). This may be an indicator that the
1147 convection is not so strong, or that may in part be a remnant. Such events may also be related to
1148 the nature of the initial formation of convection or a squall line relative to a polluted airmass.
1149 The origin of the convection, whether from a coastal ejection event or a large convective system,



1150 may play a role. Or, steering winds and wind shear are such that some moisture convergence
1151 occurs on the leading edge of an ejection event leading to weak convection along the boundary.
1152 However, this situation thus far has not been observable from satellite.

1153 To speculate, these events of thick aerosol plumes behind convection seem to be consistent with
1154 a land breeze origin that was propagated much further than normal by the monsoonal flows.
1155 Certainly the temperature change and high aerosol loading behind a cloud top front matches
1156 aircraft observations of large land breeze ejection events in the Arabian Gulf (e.g., Reid et al.,
1157 2008). In the MC case, cloud development along land breeze fronts is much larger, leading to
1158 significant convection offshore of islands (e.g., Liberti et al., 2001; Qian 2008; Virts et al., 2013).

1159 While the propagation of such land breeze fronts in a strong monsoonal flow cannot be observed
1160 by satellite due to the collinear presence of cirrus, dramatic events when the monsoonal flow is
1161 weak are frequently observed in imagery. Some examples of the Sarawak Borneo coast are
1162 presented in Figure 12, which were observed by Terra MODIS Sept 22nd and October 1st and 3rd
1163 2012. During these periods monsoonal winds slackened somewhat before and after the passing
1164 of TC Jelawat to the east. The land breeze fronts are visible as clear areas just offshore of the
1165 island, with a long cloud border parallel to the island, which in geostationary data is propagating
1166 outward. Within the imagery, heavy aerosol loadings are visible within the land breeze zone,
1167 although currently none of operational satellite aerosol products can conduct a retrieval three due
1168 to off colored ocean surface and the presence of thin cirrus. Based on MOD06 cloud products,
1169 clouds along the leading boundary are generally low, with top at ~2-3 km, with periodic cells to
1170 the 0°C melting level. It is likely that such deep warm deep clouds are precipitating-but it is
1171 unknown for sure. Occasionally, cumulonimbus with tops to 14 km are visible, in good
1172 agreement with the climatology of Virts et al., (2013). Such storms are visible based on the
1173 telltale cirrus blowing off to the southwest. Certainly these are precipitating clouds, and large
1174 enough to generate their own cold pools and may also explain the temperature drops associated
1175 with aerosol event arrival as well as help sustain the line of convection. These three events all
1176 have the same overall phenomenon observed on the Vasco; namely, an aerosol front behind a thin
1177 line of convection, some of which precipitating. The question is, once monsoon flow are
1178 enhanced, are these the phenomenon the ones ultimately responsible for the aerosol fronts



1179 observed on the Vasco. A next step for this science tem is to then attempt to model such
1180 phenomenon.

1181

1182

1183 6.0 CONCLUSIONS

1184 This paper provides an overview of the meteorological and aerosol environment measured by the
1185 *M/Y Vasco*, which sampled Maritime Continent air in September 2012 along the entire length of
1186 the Palawan Archipelago, Philippines. This cruise was a longer follow-on to a similar research
1187 cruise the previous year (Reid et al., 2015) and was a significant component of the 2012 7
1188 Southeast Asian Studies (7SEAS) southwest monsoon intensive period-a high water mark for
1189 observations throughout the Maritime Continent. The Palawan region for this research cruise
1190 was selected for being a receptor of smoke and anthropogenic emissions from Borneo, Sumatra
1191 and the Malay Peninsula as emissions were advected by southwesterly monsoonal flow into the
1192 seasonal monsoonal trough east of the Philippines. Also presented in this manuscript for context
1193 is an overview of the 2012 Maritime Continent burning season, and its relationship to key
1194 meteorological features, including ENSO, monsoonal flows, the MJO and tropical cyclones. The
1195 key conclusions of this study are as follows:

1196 1) 2012 exhibited slightly above-average burning activity in the Maritime Continent,
1197 consistent with a warm-neutral ENSO phase. Several pulses of burning and emissions occurred
1198 monthly in June through October, consistent with the migration of three moderate to weak MJO
1199 events. Particularly strong pulses were associated with large-scale upper tropospheric
1200 subsidence and regional flow enhancement provided by the inflow arms of tropical cyclones.
1201 This and previous work point to the close coupling between tropical waves and the regional
1202 aerosol system. Aerosol Optical Thickness (AOT) from AERONET sites frequently registered
1203 above 1 at 500 nm in source regions, with the strongest long-range events reaching 0.34 in
1204 Mindanao.

1205 2) The 2012 cruise home ported at Manila, Philippines, and sampled three major regions: (a)
1206 the upper Palawan chain and El Nido for September 4-13, 2012; (b) the southern Palawan chain
1207 and Balabac Island on the southern tip of the Palawan chain, ~100 km north of the northern tip of
1208 Borneo, Sept 14-20; and (c) the Sulu Sea and Tubbataha Reef Sept 21-29, 2012. In the northern



1209 locations, the atmosphere was under the influence of an easterly wave, bringing unseasonable
1210 north-to-northeasterly winds and air from the northern Philippine islands of Luzon and Mindoro.
1211 Observations included a pronounced particle nucleation event in relatively clean conditions in a
1212 region where ion mediated nucleation was predicted by Yu et al., (2008). In the southern and
1213 Sulu Sea locations, biomass burning and anthropogenically-polluted air masses were sampled,
1214 largely modulated by enhancement in monsoonal flows associated with two category 5 tropical
1215 cyclones. Fine particle concentrations reached $\sim 35 \mu\text{g m}^{-3}$, and CO was as high as 250 ppbv.
1216 Finally, while transiting through Puerto Princesa for supplies, the city plume was also sampled,
1217 including a second nucleation event in more polluted conditions with CN concentrations of
1218 $10,000 \text{ cm}^{-3}$. In comparison, “background” values of aerosol particle concentrations were on the
1219 order of 500 cm^{-3} , roughly 50-100% higher than the 2011 cruise period.

1220 3) The large-scale relationships between aerosol emissions, aerosol transport and regional
1221 meteorology during the cruise broadly matched the conceptual models of Reid et al. (2012)
1222 regarding relationships to the MJO and tropical cyclones. However, easterly waves resulted in
1223 significant weakening of the monsoonal flow, and two slow moving category 5 tropical cyclones
1224 located southeast of the Philippines resulted in monsoonal winds that had anomalous northerly
1225 and enhanced westerly components at times.

1226 4) While a multi-day biomass burning event was observed mid-cruise, in comparison to
1227 2011, aerosol events showed much higher frequency behavior. Even in the middle of the Sulu
1228 Sea, pulses of aerosol particles on the order of 3-6 hours were observed. This behavior is likely
1229 in part due to influence of scattered convection, leaving pockets of polluted and clean air masses.
1230 In addition, the aforementioned nucleation events and urban plumes added additional high-
1231 frequency signals. This high frequency behavior further complicates an already complex aerosol
1232 and cloud system.

1233 5) Finally, the 2011 cruise pointed to the important role of organized squall lines and cold
1234 pools in scavenging aerosol particles from the marine boundary layer. While very clean air was
1235 observed behind the squall lines, there were many cases where the opposite relationship was
1236 observed. That is, a rapid temperature drop and spike in wind heralded not clean air behind a
1237 squall line, but highly polluted air following behind. This difference may be a result of squall
1238 line origin, meteorology, and/or lifecycle. Some of the effects may be a result of remnant cold
1239 pools. Or, steering winds and wind shear are such that some moisture convergence occurs on



1240 the leading edge of an ejection event leading to weaker convection along the boundary.
1241 However, our prevailing hypothesis is that these events are a result of convection forming from a
1242 coastal land breeze ejection event that is caught in enhanced monsoonal flows. Clearly,
1243 understanding the dynamics of aerosol particles around such organized convective features is a
1244 high priority for future work.

1245

1246 7.0 ACKNOWLEDGEMENTS

1247 Organization of this research cruise and associated land base collections required the assistance
1248 of a number of organizations, including the staff of the Office of Naval Research-Global program
1249 office and reservist unit (esp. Joseph Johnson, Blake McBride, Paul Marshall), the Manila
1250 Observatory (esp. Antonia Loyzaga and Fr. Daniel McNamara), US State Department/ Embassy
1251 in Manila (esp. Maria Theresa Villa and Dovas Saulys), and the Naval Postgraduate School (esp.
1252 Richard Lind). We are most grateful to the *Vasco* ship management and crew, operated by
1253 Cosmix Underwater Research Ltd, (esp. Luc Heymans and Annabelle du Parc). We are also
1254 grateful to the host institutions for regional AERONET site deployment and the use of derived
1255 optical thickness data herein. Authors also benefitted from conversations with Eric Maloney
1256 (CSU), Matthew Wheeler (CSIRO), and Chidong Zhang (U of Miami). Funding for this
1257 research cruise and analysis was provided from a number of sources. *Vasco* ship time
1258 procurement was provided by the NRL 6.1 Base Program via an ONR Global grant to the Manila
1259 Observatory. Funding for US scientist deployment and instrument analysis was provided by the
1260 NRL Base Program and ONR 35. Modeling analysis was provided by ONR 32. Remote sensing
1261 and model analysis was provided by the NASA Interdisciplinary Science Program. Reservist
1262 support was provided by ONR Program 38. Ground site deployments were supported by the
1263 NASA Radiation Science Program through a grant from the Southeast Asia Composition, Cloud,
1264 Climate Coupling Regional Study (SEAC⁴RS) science team. Gas chemistry was provided by the
1265 NASA Tropospheric Chemistry Program. Author JRC acknowledges the support of NASA
1266 Interagency Agreement NNG13HH10I on behalf of MPLNET and SEAC⁴RS science teams.

1267 8.0 REFERENCES:

- 1268 Akagi, S. K., Yokelson, R. J., Weidinger, C., Alvarado, M. J., Reid, J. S., Karl, T., Crouse, J.
1269 D., and Wennberg, P. O.: Emission factors for open and domestic biomass burning for
1270 use in atmospheric models, *Atmos. Chem. Phys.*, 11, 4039–4072, doi:10.5194/acp-11-
1271 4039-2011, 2011.
- 1272 Anderson, T. L., Covert, D. S., Marshall, S. F., Laucks, M. L., Charlson, R. J., Waggoner, A. P.,
1273 Ogren, J. A., Caldow, R., Holm, R. L., Quant, F. R., Sem, G. J., Wiedensohler, A.,
1274 Ahlquist, N. A., and Bates, T. S.: Performance characteristics of a high-sensitivity three
1275 wavelength, total, backscatter nephelometer, *J. Atm. Ocean Tech.*, 13, 967-986, 1996.



- 1276 Atwood, S. A., Reid, J. S., Kreidenweis, S. M., Yu, L. E., Salinas, S. V., Chew, B. N., and
1277 Balasubramanian, R.: Analysis of source regions for smoke events in Singapore for the
1278 2009 El Nino burning season, *Atmos. Environ.*, 78, 219-230, doi:
1279 10.1016/j.atmosenv.2013.04.047, 2013.
- 1280 Atwood, S. A., et. al.: Size resolved aerosol and cloud condensation nuclei (CCN) properties in
1281 the remote South China Sea: Measurement and sources. To be submitted, *Atmos. Chem
1282 and Phys.* 2016.
- 1283 Beegum, S. N., Krishna Moorthy, K., Babu, S.S., Reddy, R. R., and Gopal, K. R.: Large scale
1284 modulations of spectral aerosol optical depths by atmospheric planetary waves, *Geophys.
1285 Res. Lett.*, 36, L03810, doi: 10.1029/2008GL036509, 2009.
- 1286 Betha, R., Spracklen, D. V., and Balasubramanian, R.: Observations of new aerosol particle
1287 formation in a tropical urban atmosphere, *Atmos. Environ.*, 71, 340-351,
1288 doi:10.1016/j.atmosenv.2013.01.049, 2013.
- 1289 Brines, M., Dall'Osto, M., Beddows, D. C. S., Harrison, R. M., Gómez-Moreno, F., Núñez, L.,
1290 Artíñano, B., Costabile, F., Gobbi, G. P., Salimi, F., Morawska, L., Sioutas, C., and
1291 Querol, X.: Traffic and nucleation events as main sources of ultrafine particles in high-
1292 insolation developed world cities, *Atmos. Chem. Phys.*, 15, 5929-5945, doi:10.5194/acp-
1293 15-5929-2015, 2015.
- 1294 Bond, T. C., Anderson, T. L., and Campbell, D.: Calibration and intercomparison of filter based
1295 measurements of visible light absorption by aerosols, *Aerosol Sci. Tech.*, 30, 582-600,
1296 doi:10.1080/027868299304435, 1999.
- 1297 Boy, M., Karl, T., Turnipseed, A., Mauldin, R. L., Kosciuch, E., Greenberg, J., Rathbone, J.,
1298 Smith, J., Held, A., Barsanti, K., Wehner, B., Bauer, S., Wiedensohler, A., Bonn, B.,
1299 Kulmala, M., and Guenther, A.: New particle formation in the Front Range of the
1300 Colorado Rocky Mountains, *Atmos. Chem. Phys.*, 8, 1577-1590, doi:10.5194/acp-8-
1301 1577-2008, 2008.
- 1302 Cahill, T. A., Goodart, C., Nelson, J. W., Eldred, R. A., Nasstrom, J. S., and Feeny, P. J.: Design
1303 and evaluation of the DRUM impactor, in: *Proceedings of the International Symposium
1304 on Particulate and Multiphase Processes*, Ariman, T. and Veziroglu, T. N. (Eds.),
1305 Hemisphere Publishing Corporation, Washington, D. C., 319-325, 1985
- 1306 Campbell, J. R., Ge, C., Wang, J., Welton, E. J., Bucholtz, A., Hyer, E. J., Reid, E. A., Chew, B.
1307 N., Liew, S.-C., Salinas, S. V., Lolli, S., Kaku, K. C., Lynch, P., Mahamud, M.,
1308 Mohamad, M., and Holben, B. N.: Applying advanced ground-based remote sensing in
1309 the Southeast Asian Maritime Continent to characterize regional proficiencies in smoke
1310 transport modeling, *J. Appl. Meteorol. Clim.*, 55, 3-22, doi:10.1175/JAMC-D-15-0083.1.,
1311 2016.
- 1312 Campbell, J. R., Reid, J. S., Westphal, D. L., Zhang, J., Tackett, J. L., Chew, B. N., Welton, E. J.,
1313 Shimizu A., and Sugimoto, N.: Characterizing aerosol particle composition and the
1314 vertical profile of extinction and linear depolarization over Southeast Asia and the
1315 Maritime Continent: the 2007-2009 view from CALIOP., *Atmos. Res.*, 122, 520-543,
1316 doi:10.1016/j.atmosres.2012.05.007, 2013.
- 1317 Chang, C.-P., Wang, Z., Mcbride, J., and Liu, C.-H.: Annual cycle of Southeast Asia-Maritime
1318 Continent rainfall and asymmetric monsoon transition, *J. Climate*, 18, 287-301, 2005.
- 1328 Chen, S. S. and Houze, R. A.: Diurnal variation and life-cycle of deep convective systems over
1329 the tropical Pacific warm pool, *Q. J. Roy. Meteor. Soc.*, 123, 357-388, 1997.



- 1330 Chew, B. N., Campbell, J. R., Reid, J. S., Giles, D. M., Welton, E. J., Salinas, S. V., and Liew, S.
1331 C.: Tropical cirrus cloud contamination in sun photometer data, *Atmos. Environ.*, 45,
1332 6724–6731, doi:10.1016/j.atmosenv.2011.08.017, 2011.
- 1333 Chew, B. N., Campbell, J. R., Salinas, S. V., Chang, C. W., Reid, J. S., Welton, E. J., Holben, B.
1334 N., and Liew, S. C.: Aerosol particle vertical distributions and optical properties over
1335 Singapore, *Atmos. Environ.*, 79, 599–613, doi:10.1016/j.atmosenv.2013.06.026, 2013.
- 1336 Chow, J. C., Watson, J. G., Pritchett, L. C., Pierson, W. R., Frazier, C. A., and Purcell, R. G.: The
1337 DRI thermal/optical analysis system: Description, evaluation and applications in U.S. air
1338 quality studies, *Atmos. Environ.*, 27A, 1185–1201, 1993.
- 1339 Cheung, H. C., Morawska, L., and Ristovski, Z. D.: Observation of new particle formation in
1340 subtropical urban environment, *Atmos. Chem. Phys.*, 11, 3823–3833, doi:10.5194/acp-11-
1341 3823-2011, 2011.
- 1342 Colman, J. J., Swanson, A. L., Meinardi, S., Sive, B. B., Blake, D. R., and Rowland, F. S.:
1343 Description of the analysis of a wide range of volatile compounds in whole air samples
1344 collected during PEM-Tropics A and B, *Anal. Chem.*, 73, 3723–3731, 2001.
- 1345 Covert, D. S., Kapustin, V. N., Quinn, P. K., Bates, T. S.: New particle formation in the marine
1346 boundary layer, *J. Geophys. Res.*, 97, 20581–20589, 1992.
- 1347 Cook, B. I. and Buckley, B. M.: Objective determination of monsoon season onset, withdrawal,
1348 and length, *J. Geophys. Res.*, 114, D23109, doi:10.1029/2009JD012795, 2009.
- 1349 Cruz, F. T., Narisma, G. T., Villafuerte, M. Q., Cheng Chua, K. U., and Olaguera, L. M.: A
1350 climatological analysis of the southwest monsoon rainfall in the Philippines, *Atmos. Res.*,
1351 122, 609–616, doi:10.1016/j.atmosres.2012.06.010, 2013.
- 1352 Draxler, R. R.: HYSPLIT4 users' guide 2004, <http://purl.access.gpo.gov/GPO/LPS47020>, last
1353 access: March 2012.
- 1354 Draxler, R. R. and Hess, G. D.: Description of the HYSPLIT_4 modeling system. NOAA Tech.
1355 Memo. ERL ARL-224, NOAA Air Resources Laboratory, Silver Spring, MD, 24 pp.,
1356 1997
- 1357 Draxler, R.R. and Hess, G.D.: An overview of the HYSPLIT_4 modeling system of trajectories,
1358 dispersion, and deposition, *Aust. Meteorol. Mag.*, 47, 295–308, 1998.
- 1359 Field, R.D. and Shen, S.S.P.: Predictability of carbon emissions from biomass burning in
1360 Indonesia, *J. Geophys. Res.*, 113, G04024, doi:10.1029/2008JG000694, 2008.
- 1361 Ge, C., Wang, J., and Reid J. S.: Mesoscale modeling of smoke transport over the Southeast
1362 Asian Maritime Continent: coupling of smoke direct radiative feedbacks below and
1363 above the low-level clouds, *Atmos. Chem. Phys.*, 14, 159–174, doi:10.5194/acp-14-159-
1364 2014, 2014.
- 1365 Giorgi, F., Coppola, E., Solomon, F., Mariotti, L., Sylla, M. B., Bi, X., Elguindi, N., Diro, G. T.,
1366 Nair, V., Giuliani, G., Turuncoglu, U. U., Cozzini, S., Guttler, I., O'Brien, T. A., Tawfik,
1367 A. B., Shalaby, A., Zakey, A. S., Steiner, A. L., Stordal, F., Sloan, L. C., Brankovic, C.:
1368 RegCM4: model description and preliminary tests over multiple CORDEX domains,
1369 *Climate Research*, 52, 7–29, 2012
- 1370 Holben, B. N., Eck, T. F., Slutsker, I., Tanre, D., Buis, J. P., Setzer, A., Vermote, E., Reagan, J. A.,
1371 Kaufman, Y. J., Nakajima, T., Lavenu, F., Jankowiak, I., and Smirnov, A.: AERONET -
1372 A federated instrument network and data archive for aerosol characterization, *Remote
1373 Sens. Environ.*, 66, 1–16, 1998.
- 1374 Hogan, T.F. and Rosmond, T.E., The description of the U.S. Navy Operational Global
1375 Atmospheric Prediction System's spectral forecast model, *Mon. Wea. Rev.*, 119, 1786–



- 1376 1815, 1991.
- 1377 Hu, L, Millet, D. B., Baasandorj, M., Griffis, T. J., Turner, P., Helmig, D., Curtis, A. J., and
- 1378 Hueber, J.: Isoprene emissions and impacts over an ecological transition region in the
- 1379 U.S. Upper Midwest inferred from tall tower measurements, *J. Geophys. Res. Atmos.*,
- 1380 120, 3553–3571, doi: 10.1002/2014JD022732, 2015.
- 1381 Hyer, E. J. and Chew, B. N.: Aerosol transport model evaluation of an extreme smoke episode
- 1382 in Southeast Asia, *Atmos. Environ.*, 44, 1422-1427, doi:10.1016/j.atmosenv.2010.01.043,
- 1383 2010.
- 1384 Hyer, E. J., Reid, J. S., Prins, E. M., Hoffman, J. P., Schmidt, C. C., Miettinen, J. I., and Giglio,
- 1385 L.: Patterns of fire activity over Indonesia and Malaysia from polar and geostationary
- 1386 satellite observations, *Atmos. Res.*, 122, 504-519, doi:10.1016/j.atmosres.2012.06.011,
- 1387 2013.
- 1388 Jamandre, C. A. and Narisma, G. T.: Spatio-temporal validation of satellite-based rainfall
- 1389 estimates in the Philippines, *Atmos. Res.*, 122, 599-608. doi:
- 1390 10.1016/j.atmosres.2012.06.024., 2013.
- 1391 Joyce, R. J., Janowiak, J. E., Arkin, P. A., and Xie, P.: CMORPH: A method that produces global
- 1392 precipitation estimates from passive microwave and infrared data at high spatial and
- 1393 temporal resolution, *J. Hydrometeorol.*, 5, 487-503, 2004.
- 1394 Kaku, K., Reid, J. S., Reid, E. A., Ross-Langerman, K., Piketh, S., Cliff, S., Al Mandoos, A.,
- 1395 Broccardo, S., Zhao, Y., Zhang, J., Perry, K. D.: Investigation of the relative fine and
- 1396 coarse mode aerosol loadings and properties in the Southern Arabian Gulf region, *Atmos.*
- 1397 *Res.*, 169, 171-182, doi:10.1016/j.atmosres.2015.09.029, 2015.
- 1398 Kanawade, V. P., Tripathi, S. N., Siingh, D., Gautam, A. S., Srivastava, A. K., Kamra, A. K.,
- 1399 Soni, V. K., Sethi, V.: Observations of new particle formation at two distinct Indian
- 1400 subcontinental urban locations, *Atmos. Environ.*, 96, 370-379,
- 1401 doi:10.1016/j.atmosenv.2014.08.001, 2014.
- 1402 Kulmala, M., Vehkamäki, H., Petaja, T., Dal Maso, M., Lauri, A., Kerminen, V.-M., Birmili, W.,
- 1403 and McMurry, P. H.: Formation and growth rates of ultrafine atmospheric particles: a
- 1404 review of observations, *J. Aerosol Sci.*, 35, 143-176, 2004.
- 1405 Levy, R. C., Mattoo, S., Munchak, L. A., Remer, L. A., Sayer, A. M., Patadia, F., and Hsu, N. C.:
- 1406 The Collection 6 MODIS aerosol products over land and ocean, *Atmos. Meas. Tech.*, 6,
- 1407 2989-3034, doi:10.5194/amt-6-2989-2013, 2013.
- 1408 Liberti, G. L., Chérüy, F., and Desbois, M.: Land effect on the diurnal cycle of clouds over the
- 1409 TOGA COARE area, as Observed from GMS IR Data. *Mon. Wea. Rev.*, **129**, 1500–1517,
- 1410 2001.
- 1411 Lin, N.-H. et al., (2013), An overview of regional experiments on biomass burning aerosols and
- 1412 related pollutants in Southeast Asia: From BASE-ASIA and the Dongsha Experiment to
- 1413 7-SEAS, *Atmospheric Environment*, 78, 1-19.
- 1414 Lynch, P., Reid, J. S., Westphal, D. L., Zhang, J., Hogan, T. F., Hyer, E. J., Curtis, C. A., Hegg,
- 1415 D. A., Shi, Y., Campbell, J. R., Rubin, J. I., Sessions, W. R., Turk, F. J., Walker, A. L.:
- 1416 Development studies towards an 11-year global gridded aerosol optical thickness
- 1417 reanalysis for climate and applied applications, *Geosci. Model Dev. Discuss.*, 8, 10455-
- 1418 10538, doi:10.5194/gmdd-8-10455-2015, 2015
- 1419 Mäkelä, J. M., Aalto, P., Jokinen, V., Pohja, T., Nissinen, A., Palmroth, S., Markkanen, T.,
- 1420 Seitsonen, K., Lihavainen, H., Kulmala, M.: Observations of ultrafine aerosol particle
- 1421 formation and growth in boreal forest, *Geophys. Res. Lett.*, 24, 1219-1222, 1997.



- 1422 Maloney, E. D. and Hartman, D. L.: The Madden Julian oscillation, barotropic dynamics, and
1423 the North Pacific tropical cyclone formation, part 1: Observations, *J. Atmos. Sci.*, 58,
1424 2545-2558, 2001.
- 1425 McGaughey, G. R., Desai, N. R., Allen, D. T., Seila, R. L., Lonneman, W. A., Fraser, M. P.,
1426 Harley, R. A., Pollack, A. K., Ivy, J. M., Price, J. H.: Analysis of motor vehicle emissions in
1427 a Houston tunnel during the Texas Air Quality Study 2000, *Atmos. Environ.*, 38, 3363-3372,
1428 doi:10.1016/j.atmosenv.2004.03.006, 2004.
- 1429 Miller, S. D., Hawkins, J. D., Kent, J., Turk, F. J., Lee, T. F., Kuchiauskas, A. P., Richardson, K.,
1430 Wade, R. and Hoffman, C.: NexSat: Previewing NPOESS/VIIRS imagery capabilities,
1431 *Bull. Amer. Meteor. Soc.*, 87, 433-446, doi: 10.1175/BAMS-87-4-433, 2006.
- 1432 Misra, V. and Li, H.: The seasonal predictability of the Asian summer monsoon in a two tiered
1433 forecast system, *Clim. Dynam.*, 42, 2491-2507, doi:10.1007/s00382-013-1838-1, 2014.
- 1434 Moore, R. M. and Zafiriou, O. C.: Photochemical production of methyl iodide in seawater, *J.*
1435 *Geophys. Res.*, 99, 16415-16420, doi: 10.1029/94JD00786, 1994.
- 1436 Moron, V., Robertson, A. W., and Beer, R.: Spatial coherence and seasonal predictability of
1437 monsoon onset over Indonesia, *J. Climate*, 22, 840-850, 2009.
- 1438 Nichol, J.: Smoke haze in Southeast Asia: A predictable recurrence, *Atmos. Environ.*, 32, 2715-
1439 2716, 1998.
- 1440 O'Neill, N. T., Eck, T. F., Smirnov, A., Holben, B. N., and Thulasiraman, S.: Spectral
1441 discrimination of coarse and fine mode optical depth, *J. Geophys. Res.*, 108, 4559, doi:
1442 10.1029/2002JD002975, 2003.
- 1443 Peatman, S. C., Mathews, A. J., and Stevens, D. P.: Propagation of the Madden-Julian
1444 Oscillation through the Maritime Continent and scale interaction with the diurnal cycle of
1445 precipitation, *Q. J. Roy. Meteor. Soc.*, 140, 814-825, doi:10.1002/qj.2161, 2014.
- 1446 Petters, M. D. and Kreidenweis, S. M.: A single parameter representation of hygroscopic growth
1447 and cloud condensation nucleus activity, *Atmos. Chem. Phys.* 7, 1961-1971, 2007.
- 1448 Petters, M. D., Carrico, C. M., Kreidenweis, S. M., Prenni, A. J., DeMott, P. J., Collett, J. L., and
1449 Moosmüller, H.: Cloud condensation nucleation activity of biomass burning aerosol, *J.*
1450 *Geophys. Res. Atmos.*, 114, D22205, doi:10.1029/2009JD012353, 2009.
- 1451 Qian, J.-H.: Why precipitation is mostly concentrated over islands in the Maritime Continent. *J.*
1452 *Atmos. Sci.*, 65, 1428-1441, doi: <http://dx.doi.org/10.1175/2007JAS2422.1>, 2008
1453
- 1454 Reid, J. S., Hobbs, P. V., Ferek, R. J., Martins, J. V., Blake, D., Dunlap, M. R., and Liousse, C.:
1455 Physical, chemical and optical properties of regional hazes dominated by smoke in
1456 Brazil, *J. Geophys. Res.*, 103, 1998.
- 1457 Reid, J. S., Koppmann, R., Eck, T. F., and Eleuterio, D. P.: A review of biomass burning
1458 emissions part II: intensive physical properties of biomass burning particles, *Atmos.*
1459 *Chem. Phys.*, 5, 799-825, 2005.
- 1460 Reid, J. S., Brooks, B., Crahan, K. K., Hegg, D. A., Eck, T. F., O'Neill, N., de Leeuw, G., Reid,
1461 E. A., and Anderson K. D.: Reconciliation of coarse mode sea-salt aerosol particle size
1462 measurements and parameterizations at a subtropical ocean receptor site, *J. Geophys.*
1463 *Res.*, 111, D02202, doi:10.1029/2005JD006200, 2006.



- 1464 Reid, J. S., Hyer, E. J., Prins, E. M., Westphal, D. L., Zhang, J. L., Wang, J., Christopher, S. A.,
1465 Curtis, C. A., Schmidt, C. C., Eleuterio, D. P., Richardson, K. A., and Hoffman, J. P.:
1466 Global Monitoring and Forecasting of Biomass-Burning Smoke: Description of and
1467 Lessons From the Fire Locating and Modeling of Burning Emissions (FLAMBE)
1468 Program, *IEEE J. Sel. Top. Appl.*, 2, 144-162, doi:10.1109/JSTARS.2009.2027443, 2009.
- 1469 Reid, J. S., S. Piketh, S., Burger, R., Ross, K., Jensen, T., R. Brintjes, Walker, A., Al Mandoos,
1470 A., Miller, S., Hsu, C., Kuciauskas, A., and D. L. Westphal., D. L.: An overview of
1471 UAE2 flight operations: Observations of summertime atmospheric thermodynamic and
1472 aerosol profiles of the southern Arabian Gulf, *J. Geophys. Res.*, 113, D14213,
1473 doi:10.1029/2007JD009435, 2008.
- 1474 Reid, J. S., Xian, P., Hyer, E. J., Flatau, M. K., Ramirez, E. M., Turk, F. J., Sampson, C. R.,
1475 Zhang, C., Fukada, E. M., and Maloney, E. D.: Multi-scale meteorological conceptual
1476 analysis of observed active fire hotspot activity and smoke optical depth in the Maritime
1477 Continent, *Atmos. Chem. Phys.*, 12, 1–31, doi:10.5194/acp-12-1-2012, 2012.
- 1478 Reid, J. S., Hyer, E. J., Johnson, R. S., Holben, B. N., Yokelson, R. J., Zhang, J., Campbell, J. R.,
1479 Christopher, S. A., Di Girolamo, L., Giglio, L., Holz, R. E., Kearney, C., Miettinen, J.,
1480 Reid, E. A., Turk, F. J., Wang, J., Xian, P., Zhao, G., Balasubramanian, R., Chew, B. N.,
1481 Janjai, S., Lagrosas, N., Lestari, P., Lin, N. H., Mahmud, M., Nguyen, A. X., Norris, B.,
1482 Oanh, N. T. K., Oo, M., Salinas, S. V., Welton, E. J., and Liew, S. C.: Observing and
1483 understanding the Southeast Asian aerosol system by remote sensing: An initial review
1484 and analysis for the Seven Southeast Asian Studies (7SEAS) program, *Atmos. Res.*, 122,
1485 403-468, doi:10.1016/j.atmosres.2012.06.005, 2013.
- 1486 Reid, J. S., Lagrosas, N. D., Jonsson, H. H., Reid, E. A., Sessions, W. R., Simpas, J. B., Uy, S.
1487 N., Boyd, T. J., Atwood, S. A., Blake, D. R., Campbell, J. R., Cliff, S. S., Holben, B. N.,
1488 Holz, R. E., Hyer, E. J., Lynch, P., Meinardi, S., Posselt, D. J., Richardson, K. A., Salinas,
1489 S. V., Smirnov, A., Wang, Q., Yu, L., and Zhang, J.: Observations of the temporal
1490 variability in aerosol properties and their relationships to meteorology in the summer
1491 monsoonal South China Sea/East Sea: the scale-dependent role of monsoonal flows, the
1492 Madden–Julian Oscillation, tropical cyclones, squall lines and cold pools, *Atmos. Chem.
1493 Phys.*, 15, 1745-1768, doi:10.5194/acp-15-1745-2015, 2015.
- 1494 Rose, D., Nowak, A., Achtert, P., Wiedensohler, A., Hu, M., Shao, M., Zhang, Y., Andreae,
1495 M.O., and Pöschl, U.: Cloud condensation nuclei in polluted air and biomass burning
1496 smoke near the mega-city Guangzhou, China – Part 1: Size-resolved measurements and
1497 implications for the modeling of aerosol particle hygroscopicity and CCN activity,
1498 *Atmos. Chem. Phys.*, 10, 3365–3383, 2010.
- 1499 Rosenfeld, D.: TRMM observed first direct evidence of smoke from forest fires inhibiting
1500 rainfall, *Geophys. Res. Lett.*, 26, 3105–3108, doi:10.1029/1999GL006066, 1999.
- 1501 Salinas, S. V., Chew, B. N., Liew, S. C.: Retrievals of aerosol optical depth and Angstrom
1502 exponent from ground based Sun-photometer data in Singapore, *Appl. Optics*, 48, 1473-
1503 1484, doi: 10.1364/AO.48.001473, 2009.
- 1504 Salinas, S. V., Chew, B. N., Mohamad, M., Mahmud, M., and Liew, S. C.: First measurements of
1505 aerosol optical depth and Angstrom exponent number from AERONET's Kuching site,
1506 *Atmos. Environ.*, 78, 231-241, doi:10.1016/j.atmosenv.2013.02.016, 2013.
- 1507 Sampson, C. R. and Schrader A. J.: The Automated Tropical Cyclone Forecasting System
1508 (Version 3.2), *Bull. Amer. Meteor. Soc.*, 81, 1231-1240, 2000.
- 1509 Seigel, R. B. and van den Heever, S. C.: Dust lofting and ingestion by supercell storms, J.



- 1510 Atmos. Sci., 69, 1453–1473, doi:10.1175/JAS-D-11-0222.1, 2012.
- 1511 Sessions, W., Reid, J. S., Benedetti, A., Colarco, P., da Silva, A., Lu, S., Sekiyama, T., Tanaka, T.,
1512 Baldasano, J., Basart, S., Brooks, M., Eck, T., Iredell, M., Hansen, J., Jorba, O., Juang,
1513 H., Lynch, P., Morcrette, J., Moorthi, S., Mulcahy, J., Pradhan, Y., Razinger, M.,
1514 Sampson, C., Wang, J., Westphal, D.: Development towards a global operational aerosol
1515 consensus: basic climatological characteristics of the International Cooperative for
1516 Aerosol Prediction Multi-Model Ensemble (ICAP-MME) Atmos. Chem. Phys., 15, 2533-
1517 2534, doi: 10.5194/acp-15-2533-2015, 2015.
- 1518 Shi, Y., Zhang, J., Reid, J. S., Holben, B., Hyer, E. J., and Curtis, C.: An analysis of the
1519 collection 5 MODIS over-ocean aerosol optical depth product for its implication in
1520 aerosol assimilation, Atmos. Chem. Phys., 11, 557–565, doi:10.5194/acp-11-557-2011,
1521 2011.
- 1522 Simpson, I. J., Aburizaiza, O. S., Siddique, A., Barletta, B., Blake, N. J., Gartner, A., Khwaja,
1523 H., Meinardi, S., Zeb, J., and Blake, D. R.: Air quality in Mecca and surrounding holy
1524 places in Saudi Arabia during Hajj: Initial survey, Environ. Sci. Technol., 48, 15, 8529-
1525 8539, 2014.
- 1526 Smirnov, A., Holben, B. N., Giles, D. M., Slutsker, I., O'Neill, N. T., Eck, T. F., Macke, A.,
1527 Croot, P., Courcoux, Y., Sakerin, S. M., Smyth, T. J., Zielinski, T., Zibordi, G., Goes, J. I.,
1528 Harvey, M. J., Quinn, P. K., Nelson, N. B., Radionov, V. F., Duarte, C. M., Losno, R.,
1529 Sciare, J., Voss, K. J., Kinne, S., Nalli, N. R., Joseph, E., Krishna Moorthy, K., Covert, D.
1530 S., Gulev, S. K., Milinevsky, G., Larouche, P., Belanger, S., Horne, E., Chin, M., Remer,
1531 L. A., Kahn, R. A., Reid, J. S., Schulz, M., Heald, C. L., Zhang, J., Lapina, K., Kleidman,
1532 R. G., Griesfeller, J., Gaitley, B. J., Tan, Q., and Diehl, T. L.: Maritime aerosol network
1533 as a component of AERONET – first results and comparison with global aerosol models
1534 and satellite retrievals, Atmos. Meas. Tech., 4, 583-597, doi:10.5194/amt-4-583-2011,
1535 2011.
- 1536 Staub, K. H., Kilandis, G. N., and Ciesielski, P. E.: The role of equatorial waves in the onset of
1537 the South China Sea summer monsoon and the demise of the El Nino during, 1998,
1538 Dynam. Atmos. Oceans, 42, 216-238, doi: 10.1016/j.dynatmoce.2006.02005, 2006.
- 1539 Suess, E.: Marine cold seeps and their manifestations: geological control, biogeochemical
1540 criteria and environmental conditions, Int. J. Earth Sci, 103, doi:10.1007/s00531-014-
1541 1010-0, 1889-1916, 2014.
- 1542 Tian, B., Waliser, D. E., Kahn, R. A., Li, Q., Yung, Y. L., Tyranowski, T., Geogdzhayev, I. V.,
1543 Mishchenko, M. I., Torres, O., Smirnov, A.: Does the Madden-Julian Oscillation
1544 influence aerosol variability?, J. Geophys. Res., 113, D12215,
1545 doi:10.1029/2007JD009372, 2008.
- 1546 Tong, H. W., Chan, J. C. L., Zhou, W.: The role of the MJO and mid-latitude fronts in the South
1547 China Sea Summer monsoon onset, Clim. Dynam., 33, 827-841, doi: 10.1007/s00382-
1548 008-0490-7, 2009.
- 1549 Virts, K., S., Wallace, J. M., Hutchins, M. L., and Holzworth, R. H.: Diurnal lightning variability
1550 over the Maritime Continent: Impact of low-level winds, cloudiness, and the MJO. *J.*
1551 *Atmos. Sci.*, **70**, 3128–3146, doi: http://dx.doi.org/10.1175/JAS-D-13-021.1, 2013.
- 1552 Wang, J., Gei, C., Yang, Z., Hyer, E., Reid, J. S., Chew, B. N., and Mahmud, M.: Mesoscale
1553 modeling of smoke transport over the South Asian maritime continent: vertical
1554 distributions and topographic effect, Atmos. Res., 122, 486-503, 2013.



- 1555 Wiedinmyer, C., Greenberg, J., Guenther, A., Hopkins, B., Baker, K., Geron, C., Palmer, P. I.,
1556 Long, B. P., Turner, J. R., Pétron, G., Harley, P., Pierce, T. E., Lamb, B., Westberg, H.,
1557 Baugh, W., Koerber, M., and Janssen, M.: Ozarks Isoprene Experiment (OZIE):
1558 Measurements and modeling of the “isoprene volcano,” *J. Geophys. Res.*, 110, D18307,
1559 doi:10.1029/2005JD005800, 2005.
- 1560 Wheeler, M. C. and Hendon, H. H.: An all-season real-time multivariate MJO index:
1561 Development of an index for monitoring and prediction, *Mon. Wea. Rev.*, 132, 1917–
1562 1932, 2004.
- 1563 Wu, P., Hara, M., Hamada, J.-I., Yamanaka, M.D., and Kimura, F.: Why a large amount of rain
1564 falls over the sea in the vicinity of western Sumatra island during nighttime. *Appl.*
1565 *Meteorol.* 48, 1345–1361. [http://dx.doi.org/ 10.1175/2009JAMC2052.1](http://dx.doi.org/10.1175/2009JAMC2052.1), 2009.
- 1566 Xian, P., Reid, J. S., Turk, J. F., Hyer, E. J., and Westphal D. L.: Impact of modeled versus
1567 satellite measured tropical precipitation on regional smoke optical thickness in an aerosol
1568 transport model, *Geophys. Res. Lett.*, 36, L16805, doi:10.1029/2009GL038823, 2009.
- 1569 Xian, P., Reid, J. S., Atwood, S. A., Johnson, R., Hyer, E. J., Westphal, D. L., and Sessions, W.:
1570 Smoke transport patterns over the Maritime Continent, *Atmos. Res.*, 122, 469-485,
1571 doi:10.1016/j.atmosres.2012.05.006, 2013.
- 1572 Yang, L., Nguyen, D. M., Jia, S. H., Reid, J. S., and Yu L. E.: Impacts of biomass burning smoke
1573 on the distributions and concentrations of C₂–C₅ dicarboxylic acids and dicarboxylates in
1574 a tropical urban environment, *Atmos. Environ.*, 78, 211-218,
1575 doi:10.1016/j.atmosenv.2012.03.049, 2013.
- 1576 Yu, F., Wang, Z., Luo, G., and Turco, R.: Ion-mediated nucleation as an important global source
1577 of tropospheric aerosols, *Atmos. Chem. Phys.*, 8, 2537-2554, doi:10.5194/acp-8-2537-
1578 2008, 2008.
- 1579 Zhang, C.: Madden-Julian Oscillation, *Rev. Geophys.*, 43, RG2003,
1580 doi:10.1029/2004RG000158, 2005.
- 1581 Zhang, C.: Madden-Julian Oscillation: Bridging Weather and Climate, *Bull. Amer. Meteor. Soc.*,
1582 94, 1849-1870, doi:10.1175/BAMS-D-12-00026.1, 2014.
- 1583 Zhang, J. L., Reid, J. S., Westphal, D. L., Baker, N. L., and Hyer, E. J.: A system for operational
1584 aerosol optical depth data assimilation over global oceans, *J. Geophys. Res. Atmos.*, 113,
1585 D10208, doi:10.1029/2007JD009065, 2008.
- 1586



Table 1. Aerosol and whole-air sample concentrations and associated particle data for key aerosol events during the study. Units are pptv unless otherwise noted. BDL=Below detectible limits. Local standard time is 8:00 ahead of UTC

Specie	Back-ground	Biomass Burning		Apo Reef			Puerto Princesa			
		Sep 14 6:38Z	Sep 26 0:52Z	Pre- Event Sept 5 22:20Z	Early Event Sept 6 2:45Z	Late Event Sept 6 7:45Z	Inside Sep 13 2:47Z	Outside Sept 19 22:55Z	In plume Sep 19 23:52Z	Depart Sep 20 22:00 Z
CN (cm ⁻³)	~400	2500	2100	490	1100	1450	>10000	400	2230	317
~PM ₁ (µg m ⁻³)	~1.5	30	21	1.2	1.8	1.9	10	1.5	8	2.5
CO (ppbv)	77+/-3	244	209	100	98	92	144	111	207	136
CH ₄ (ppmv)	1.77+/-0.01	1.77	1.76	1.768	1.81	1.77	1.77	1.94	1.82	1.82
DMS	24+/-12	27	31	7.3	19	9.1	8.6	13.2	9.8	11.1
CH ₃ I	0.7+/-0.7	1.38	1.48	0.95	0.55	2.9	0.42	1.25	0.43	0.48
Ethane	348+/-55	877	824	399	504	369	525	514	619	434
Ethene	47+/-32	376	490	101	212	69	274	381	880	235
Ethyne	68+/-18	561	501	107	131	102	315	116	953	123
Propane	67+/-33	137	166	86	90	68	140	111	374	78
Propene	24+/-12	76	148	49	80	76	62	249	236	62
i-Pentane	57+/-33	35	51	23	40	30	241	49	537	64
n-Pentane	40+/-23	26	43	18	24	19	106	50	258	56
Hexane	31+/-14	21	38	15	12	9	49	48	123	52
Benzene	32+/-27	140	162	36	40	23	96	42	198	40
Isoprene	22+/-36	4	BDL	6	3	BDL	3	18	59	14
i-PrONO ₂	1.1+/-0.3	2.3	2.7	1.7	2.0	1.4	2.2	3.1	1.9	2.6
n-PrONO ₂	0.3+/-0.2	0.4	0.4	0.3	0.2	0.5	0.5	0.2	0.3	0.6
BuONO ₂	1+/-0.7	1.6		1.3	1.6	1.2	2.7	2.1	1.9	2.0
Ratio of i to n	~1.4	1.3	1.2	1.3	1.7	1.6	2.3	1	2.08	1.2

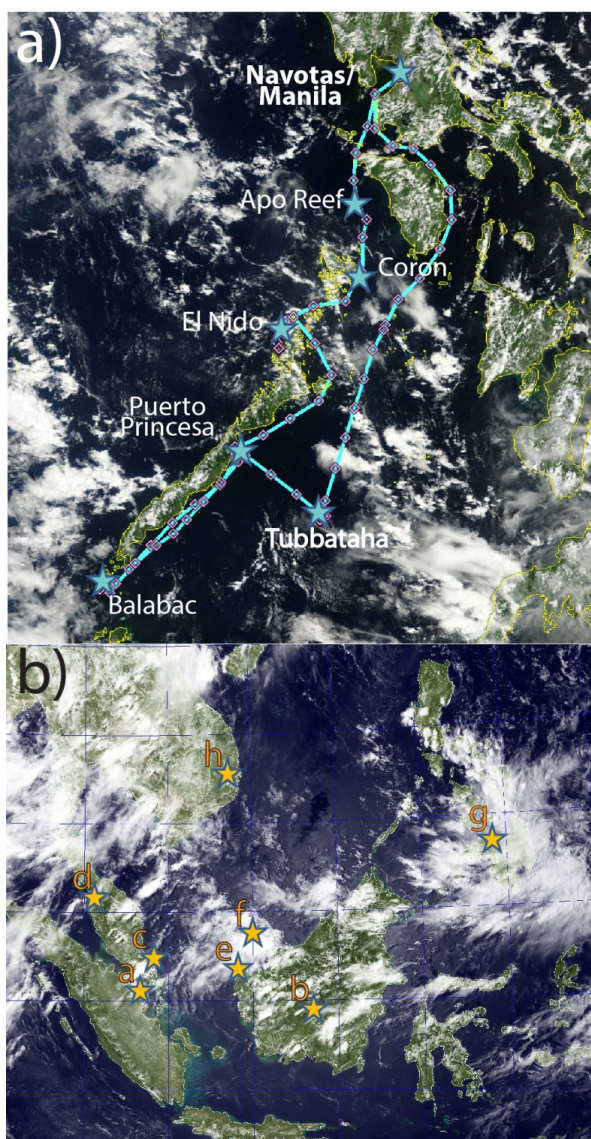


Figure 1. a) Cruise track with major sampling locations started overlaid on Terra MODIS 7 Sep 2012. b) AERONET sun photometer sites used in this analysis overlaid on MTSAT including false color visible imagery for 7 Sep 2012 6:32 UTC, a-Jambi; b-Palangkaraya; c-Singapore; d-Tahir; e-Pontianak; f- Kuching; g-Marbel University; h- Nha Trang.

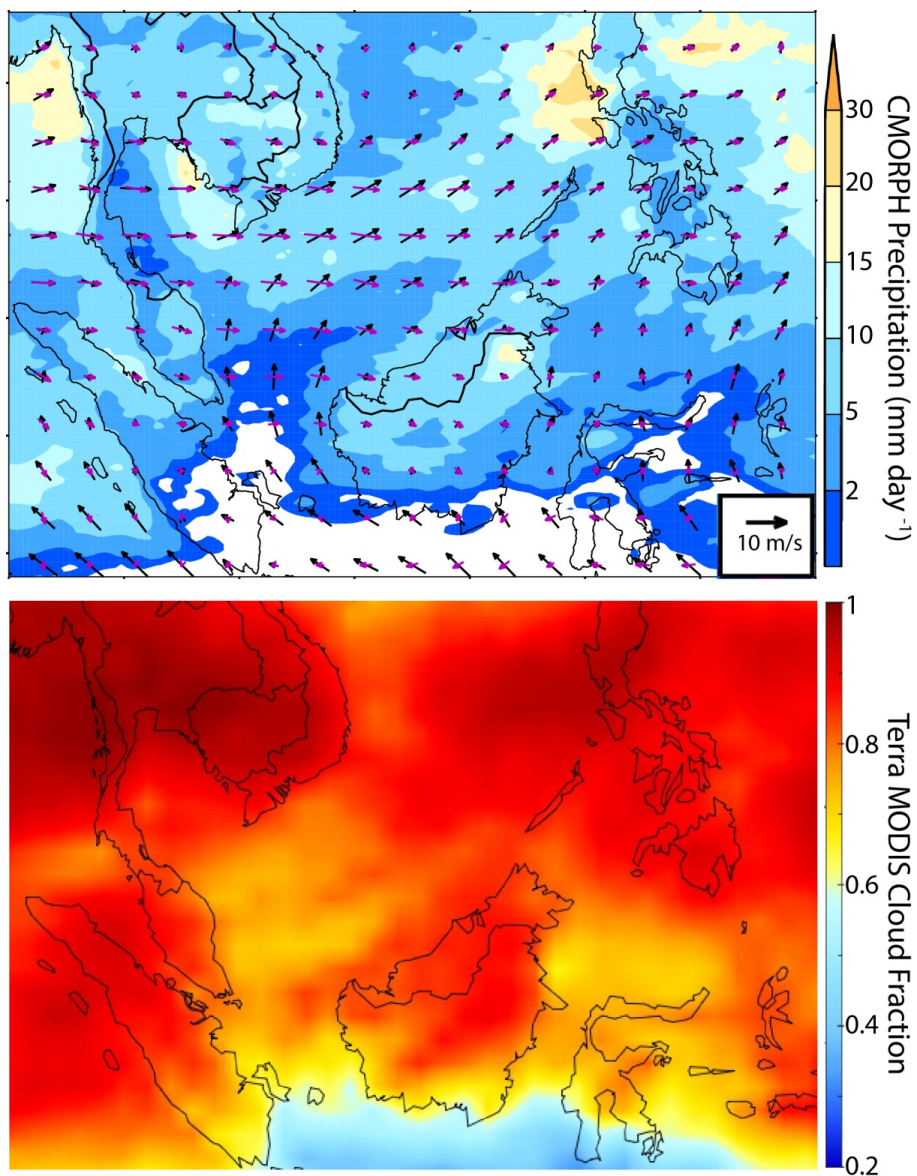


Figure 2. Average August & September 2012 NAVGEM Surface (Black) and 700 hPa (Magenta) winds overlaid on average CMORPH derived rain rate.

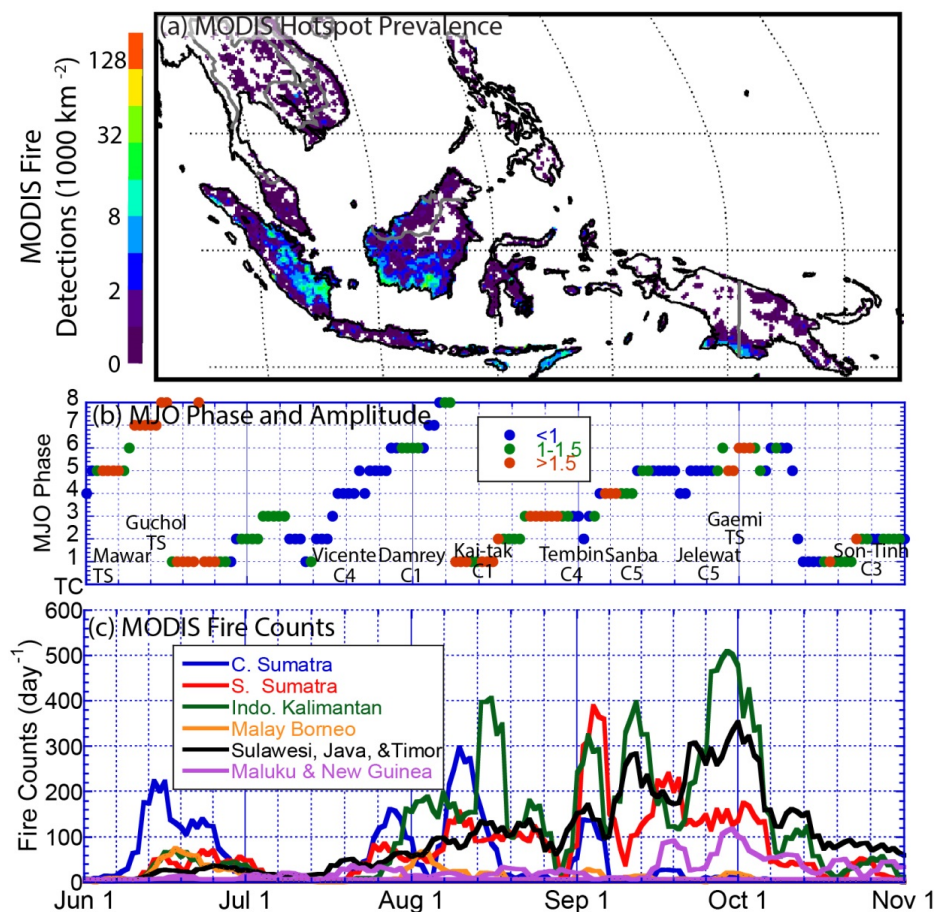


Figure 3. (a) Overall Terra and Aqua MODIS detected fire prevalence for June-October 2012; (b) Wheeler index of MJO phase and color coded amplitude. Amplitudes above one are considered statistically significant. (c) A 5 day box car average of observed Terra and Aqua combined active fire hotspot detections for the 2012 Maritime Continent burning season by region as defined in Reid et al., (2012; 2015).

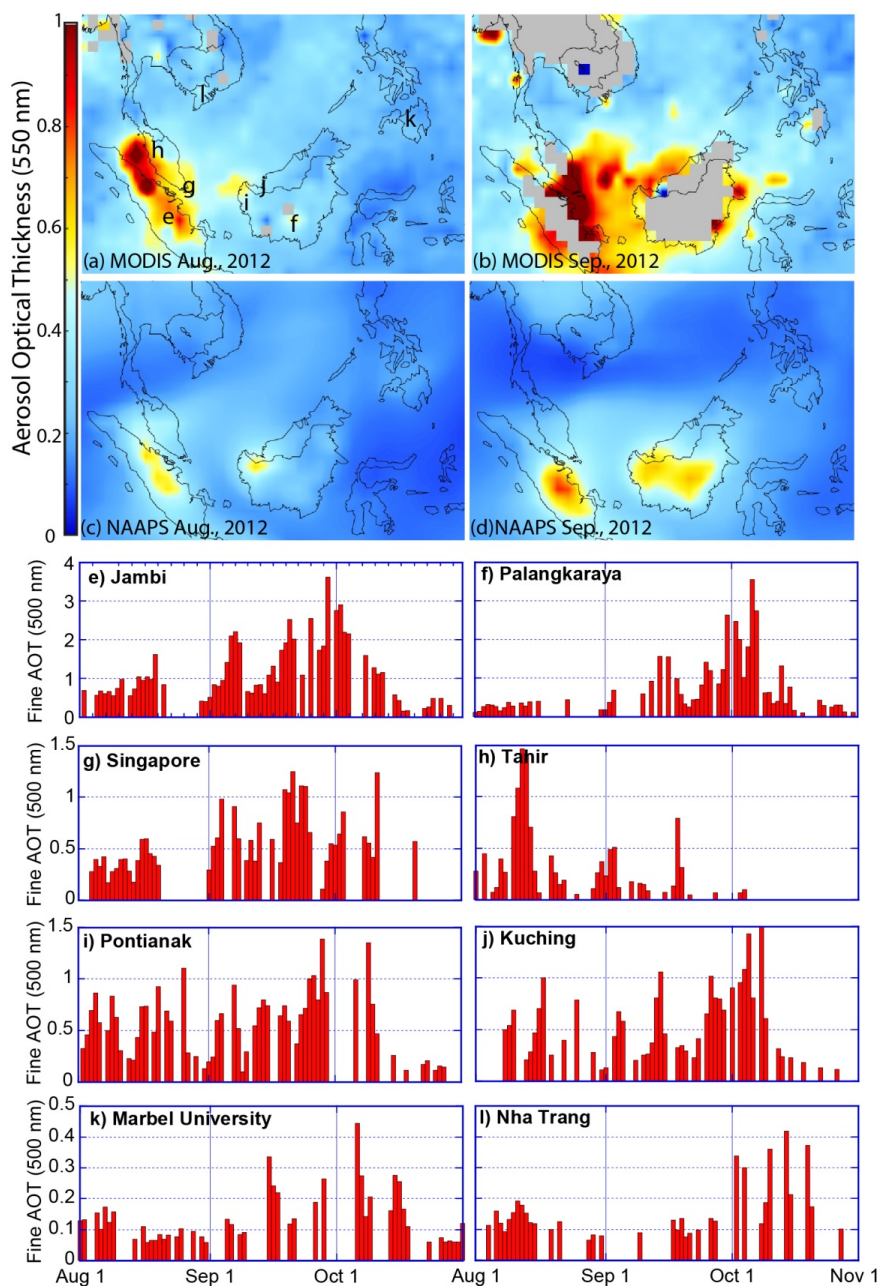


Figure 4. August and September 2012 monthly average 550 nm total Aerosol Optical Thickness (AOT) from (a) and (b) MODIS and (c) and (d) NAAPS reanalysis. Also shown are (e)-(l) daily average AERONET 500 nm fine mode AOTs. Site locations are also marked in (a).

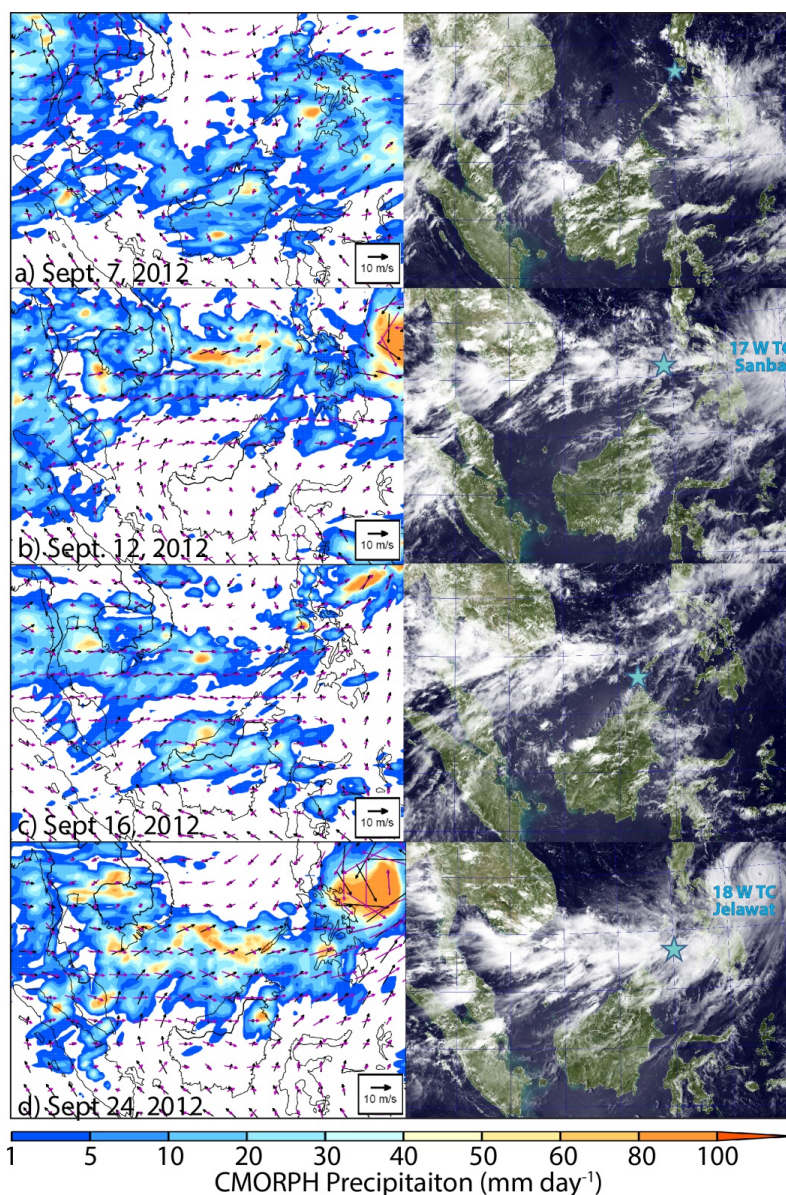


Figure 5. Model, satellite precipitation and MTSAT visible imagery for four representative days at major anchorages throughout the *Vasco* cruise. Left column provides daily averaged NAVGEM wind (black surface, magenta 700 hPa) overlaid on CMORPH daily averaged precipitation. Right column is the 02:32 UTC (nominal noon local time) MTSAT false color visible image, annotated with Vasco position (blue star) and active TCs influencing regional weather. Selected dates are at major sampling moorings/anchorages (a) Sept 7, at Apo Reef, (b) Sept 12 at El Nido, (c) Sept 16 at Balabac Island, and (d) Sep 24th at Tubbataha Reef.

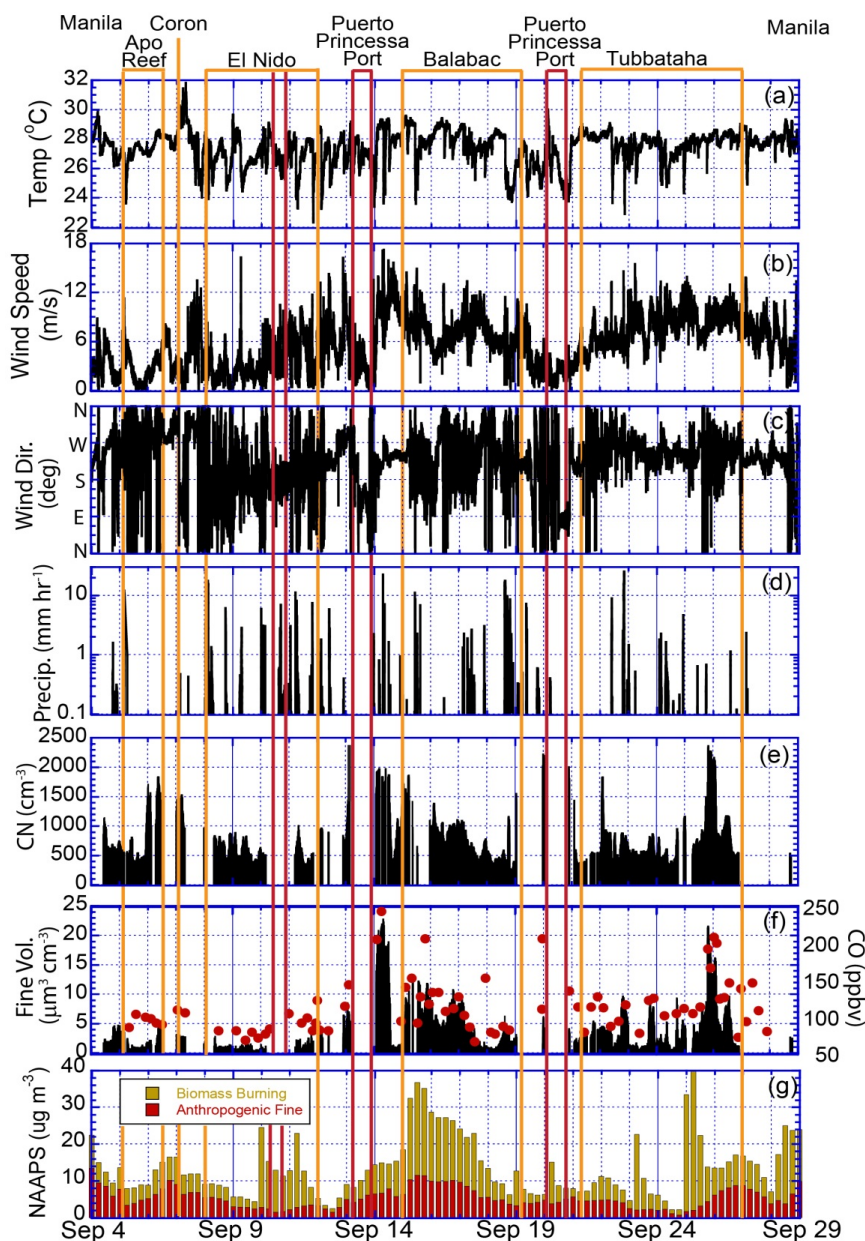


Figure 6. Time series of key meteorological and compositional data along the Vasco track (UTC Time). Locations of stationary sampling and in port periods are bound in orange and red brackets, respectively. Included are a) temperature [$^{\circ}\text{C}$]; b) wind speed [m s^{-1}]; c) wind direction; d) precipitation rate [mm hr^{-1}]; e) condensation nuclei count [cm^{-1}]; f) Fine mode volume as derived by the PCASP [black $\mu\text{m}^3 \text{cm}^{-3}$] and the gas can CO [red dots ppbv]. Also shown is the combined NAAPS model derived fine mode mass sampled along the Vasco track.

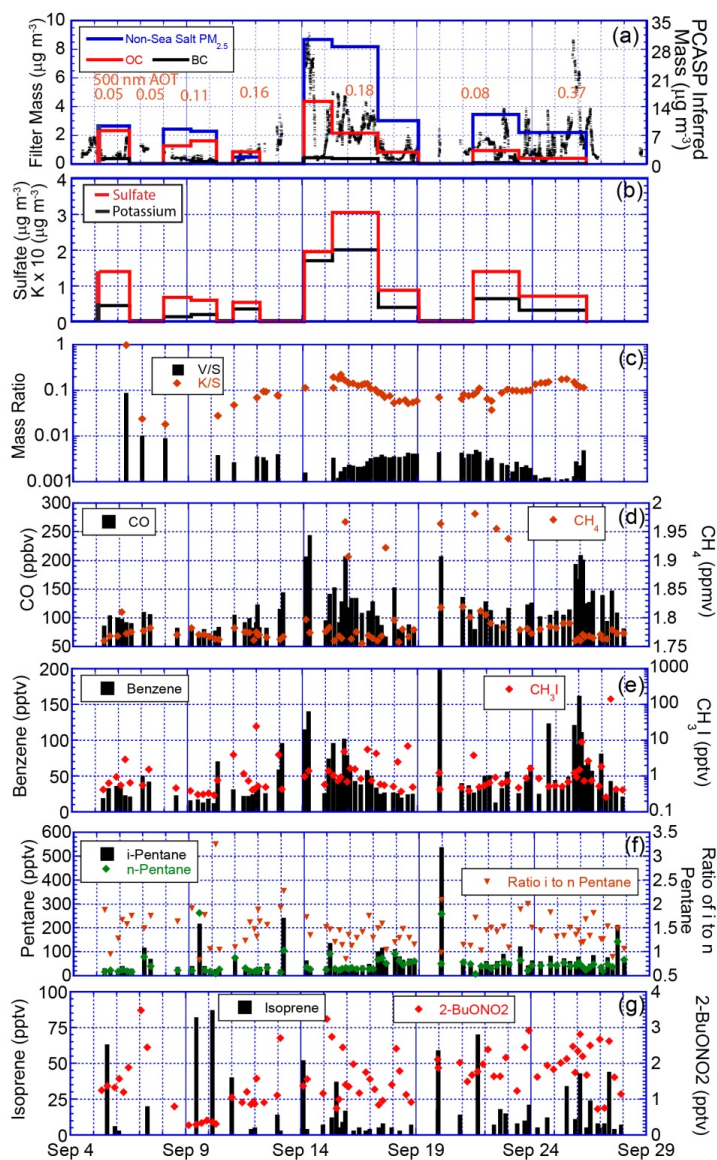


Figure 7. Time series of chemistry measurements including (a) Filter based gravimetry and Organic-OC and Black-BC carbon. Also shown is 30 minute averaged mass inferred from the PCASP; (b) filter sulfate and potassium; (c) DRUM sampler elemental ratios of vanadium and potassium to sulfur; (d) whole-air sampled CO and methane; (e) whole-air sampled benzene and methyl iodide; (f) whole-air sampled i- and n-pentane with their ratio; (g) whole-air sampled isoprene and 2-butanalkyl nitrate.

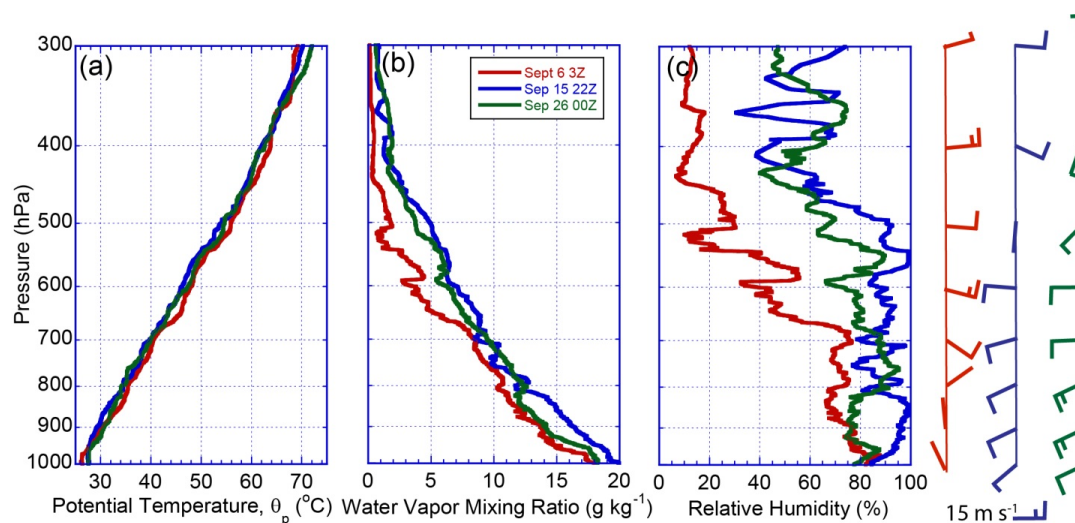


Figure 8. Sounding profiles of (a) Potential temperature; (b) Water vapor mixing ratio; and (c) Relative humidity for profiles corresponding to the nucleation event on Sept 6 at Apo reef, and the biomass burning cases of September 15 and 26th at Balabac island and Tubbataha Reef, respectively. Wind flags for these cases are marked on the far right.

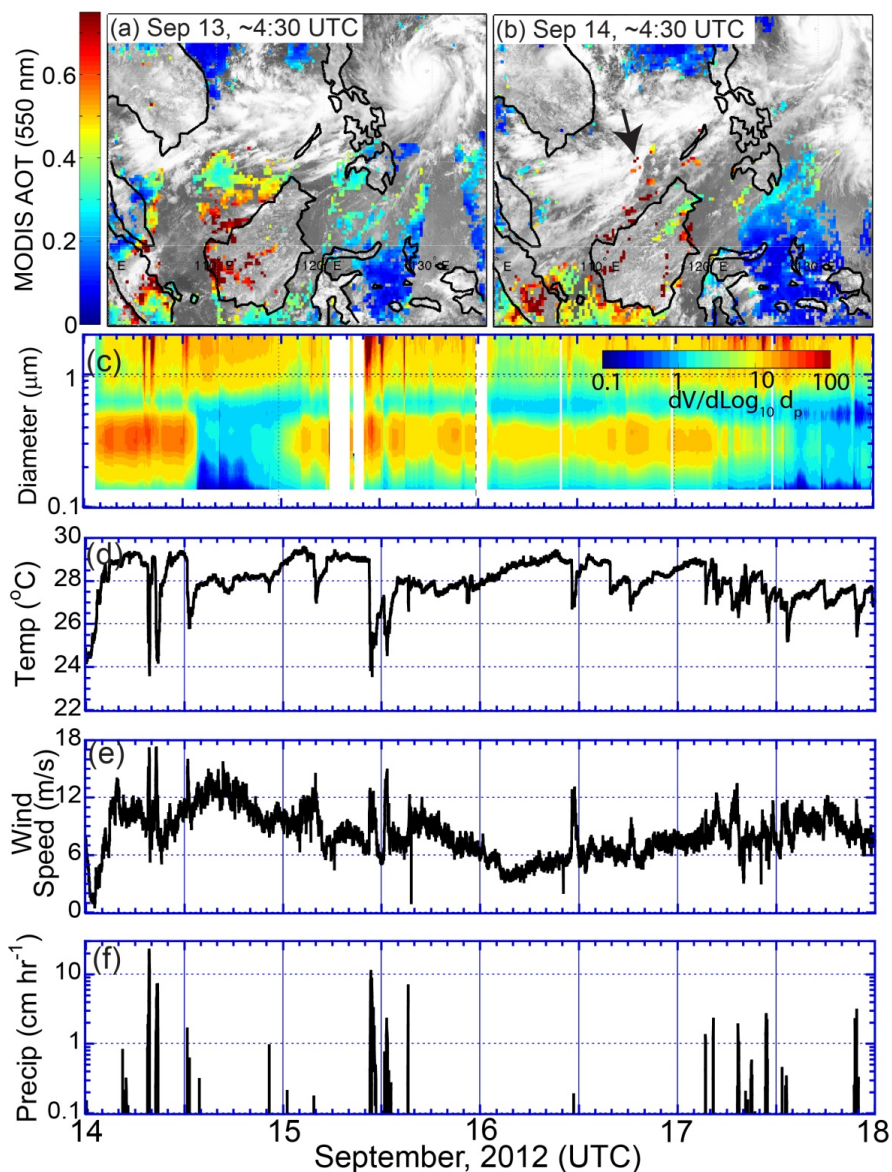


Figure 9. Satellite data and Vasco one-minute data time series describing the Sept 14-17 smoke event. (a) and (b), combined Terra and Aqua MODIS C6 550 nm AOT overlaid on MTSAT visible channel for September 13 and 14, respectively; (c) PCASP volume distribution; (d) Temperature; (e) Wind speed; (f) Precipitation rate. The presence of a large squall line originating from a massive thunderstorm over the Malaya Peninsula that resulted in the Sept 14 12Z clean period as evident in (c) is marked with an arrow in (b).

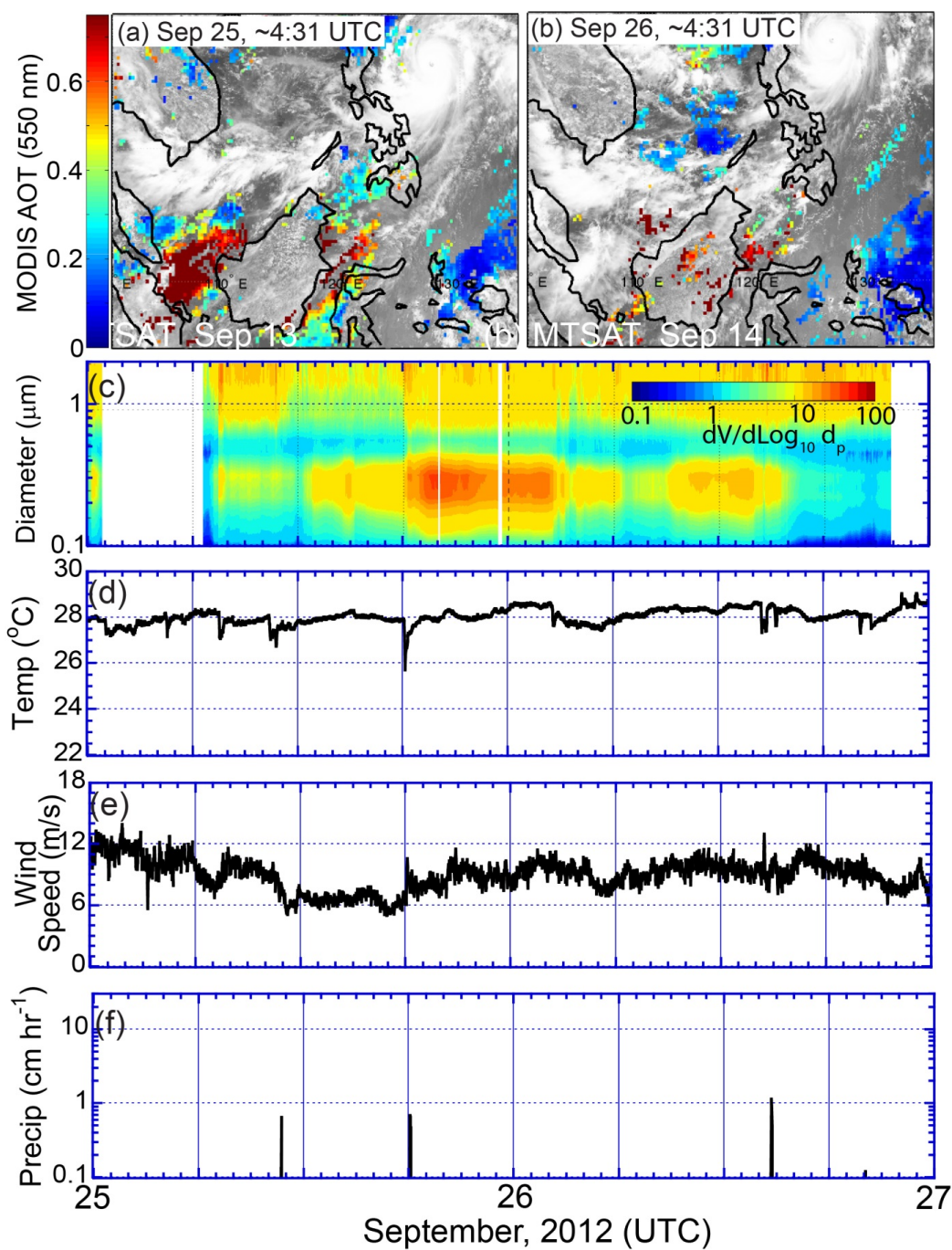


Figure 10. Same as Figure 9 but for the Sept 25-26, 2012 smoke event.

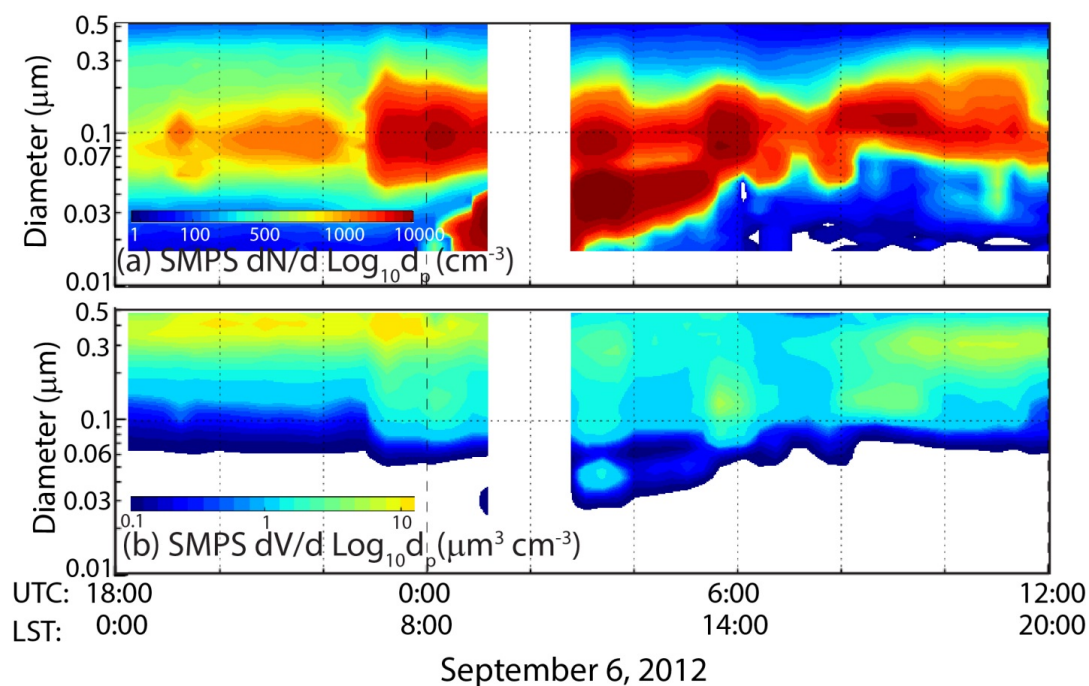


Figure 11. SMPS particle number and volume distribution for the Sept 6th nucleation event at Apo reef. Corresponding whole-air samples are listed in Table 1 including 22:20Z Sept. 5th as a pre event can, 2:45Z Sept 6th in the middle of the event, and 7:30Z Sept 6, for post event.

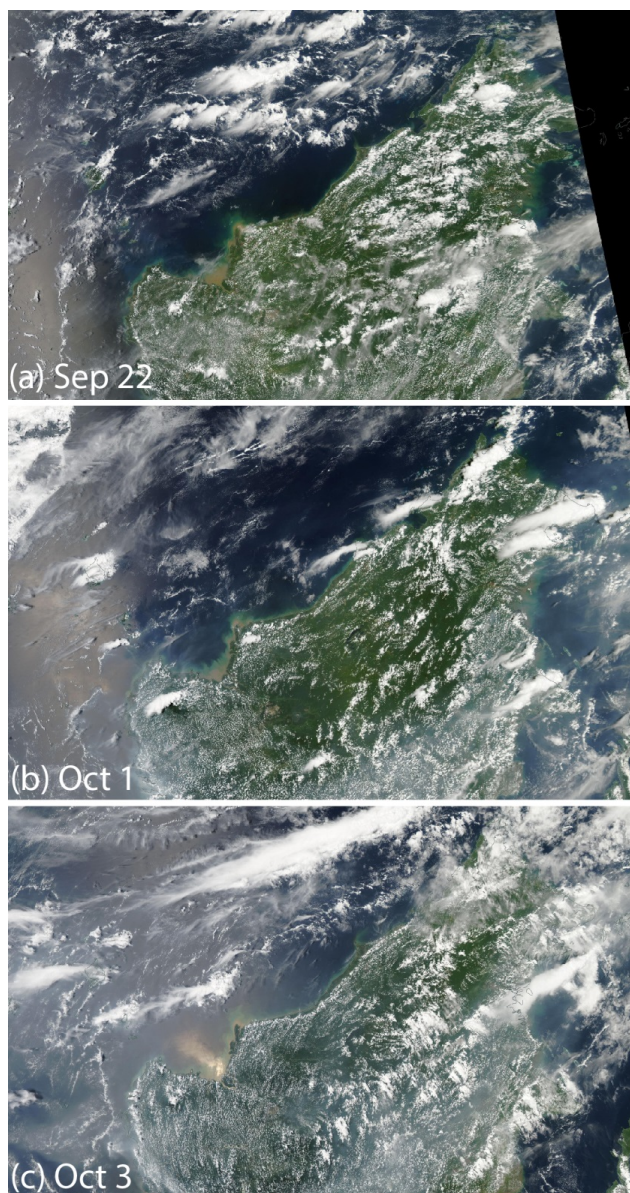


Figure 12. NASA Terra MODIS images of the northern Borneo coast off of Sarawak Malaysia demonstrating land breeze induced ejection events. Such events are identified by clear areas just offshore of the island with a leading edge of clouds. Occasionally embedded in this line of clouds are thunderstorms.